FFT-Based Numerical Method for Non-Linear Elastic Contact

Fei Guo (guof2014@mail.tsinghua.edu.cn)
State Key Laboratory of Tribology, Tsinghua University https://orcid.org/0000-0003-2416-343X
Fan Wu
State Key Laboratory of Tribology, Tsinghua University
Xinyong Li
State Key Laboratory of Smart Manufacturing for Special Vehicles and Transmission System
Yijie Huang
tate Key Laboratory of Tribology, Tsinghua University
Zhuo Wang
State Key Laboratory of Smart Manufacturing for Special Vehicles and Transmission System

Original Article

Keywords: Numerical Method, Elastoplastic Contact, Hyperelastic Contact, FEM, FFT

Posted Date: January 14th, 2021

DOI: https://doi.org/10.21203/rs.3.rs-144156/v1

FFT-Based Numerical Method for Non-Linear Elastic Contact

Fei Guo[a,b]*, Fan Wu[a,b], Xinyong Li[c], Yijie Huang[a,b], Zhuo Wang[c]

[a] *State Key Laboratory of Tribology, Tsinghua University, Beijing 100084, China*

[b] *Joint Research Center for Rubber and Plastic Seals, Tsinghua University, Beijing 100084, China*

[c] *State Key Laboratory of Smart Manufacturing for Special Vehicles and Transmission System, Baotou, Inner Mongolia, China.*

* *Corresponding author. E-mail address: guof2014@mail.tsinghua.edu.cn*

Abstract:

Based on FFT, a numerical method suitable for elastoplastic and hyperelastic frictionless contact is proposed in this paper, which can be used to solve 2D and 3D contact problems. The non-linear elastic contact problem is transformed to linear elastic contact considering residual deformation (or equivalent residual deformation). Numerical simulations for elastic, elastoplastic and hyperelastic contact between hemisphere and rigid plane are compared with the results of finite element method (FEM) to verify the accuracy of the numerical method. Compared with the existing elastoplastic contact numerical methods, the calculation efficiency is improved while ensuring a certain calculation accuracy (pressure error does not exceed 15% while calculation time does not exceed 10 minutes in a 64×64 grid). For hyperelastic contact, the proposed method reduces the dependence of the approximation result on load as in linear elastic approximation. Despite a certain error, the simplified numerical method shows a better approximation result than linear elastic contact approximation, which can be used for the fast solution in engineering applications. Finally, taking the sealing application as an example, the contact and leakage rate between 3D complicated rough surfaces are calculated.

Keywords: Numerical Method; Elastoplastic Contact; Hyperelastic Contact; FEM; FFT

1. Introduction

In the theoretical research of sealing, it is essential to calculate the contact pressure and area between asperities of sealing pair to obtain the leakage rate, which is the most effective parameter to characterize the sealing performance of sealing system [1-5]. For axisymmetric sealing structures, the contact between sealing pair is usually simplified as a two-dimensional (2D) problem. However, in some specific cases, such as the anisotropy of the sealing surface texture, the contact problem is difficult to be simplified and needed to be solved using a three-dimensional (3D) model. Metal / rubber and metal / plastic pairs are commonly used for sealing system. The deformation of rubber or plastic is mainly considered due to their smaller elastic modulus than that of metal. Unlike linear elastic contact, rubber is a hyperelastic material whose uniaxial compressive stress-strain curve is non-linear. For plastic, plastic deformation occurs when the contact pressure is too high. Therefore, it is necessary to consider whether the contact problem is a 2D or 3D problem, and whether it is a linear or non-linear elastic contact for different sealing systems, and then an appropriate contact model should be selected for calculation.

At present, the contact models are mainly divided into three categories: statistical model (such as the GW model [6] and improved models based on the GW model [7, 8], fractal model [9, 10] and deterministic model. For statistical model and fractal model, the description of rough surface is simplified using statistical parameters and fractal parameters, respectively. In addition, calculation results of both two models are obtained based on the assumption that interaction between asperities is

simplified or ignored. Compared with the former two, the deterministic model is based on the deterministic description of rough surface. More accurate pressure distribution and deformation results can be finally obtained using this model. Deterministic model can be divided into analytical model and numerical model. For analytical model, Hertz theory can be used to solve the contact area and average contact pressure of ball-plane elastic contact. Westerggard [11] derived the complete solution in closed form to the elastic contact of a one-dimensional sinusoidal surface with a flat surface. Based on Westerggard's research results, Johnson [12] extended it to a two-dimensional sinusoidal surface with a flat surface. Zhu [13] proposed an elastic-plastic model for line contact structures based on the understanding of the yield mechanism. For numerical model, one approach is to use the finite element method (FEM) to analyze the contact behavior between solids with different materials [14-16]. However, for complicated rough surface contact, especially for 3D problem, a refined mesh is needed for FEM, which would cause a long calculation time or even non-convergence. Another approach is semi-analytic method (SAM). Polonsky [17] proposed a numerical method to solve rough surface contact problems based on the multi-level multi-summation and conjugate gradient techniques. Stanley [18] solved the elastic contact between a rigid plane and a half-space based on Fast Fourier Transform (FFT) and analytical solution from Westerggard [11] and Johnson [12]. It should be noted that the interaction between asperities is considered in this method. FFT is also used in the numerical methods proposed by Johnson [12] and Wang [19]. In addition to the linear elastic contact calculation, Jacq [20], Wang [21], Chen [22] and other researchers [23, 24] proposed numerical methods for elastoplastic contact. Moreover, there are other contact models considering friction (tangential deformation) [25, 26] and heat [27, 28].

For elastoplastic contact, the current semi-analytical methods [20-22] are mainly based on purely elastic contact considering plastic deformation, in which plastic strain is calculated using the Von Mises yield criterion and specific hardening law. This kind of method involves the calculation of the stress and strain of bulk element, which can be used to analyze contact fatigue, damage and so on. However, for complicated 3D rough surface contact, large number of 3D grid elements would cause long calculation time. Therefore, it is necessary to propose a simplified method to adapt to the engineering applications. In addition, hyperelastic contact is usually simplified to linear elastic contact problem, which needs to be improved in calculation accuracy.

Based on the work of Stanley et al. [18], a numerical method suitable for elastoplastic and hyperelastic frictionless contact is proposed in this paper, which can be used to solve 2D and 3D contact problems. Compressive stress-strain curve of material with linear hardening property or hyperelastic material such as rubber is simplified to a combination of two linear segments with different slopes, and the solution of residual deformation is also simplified. The non-linear elastic contact problem is transformed to linear elastic contact considering residual deformation (or equivalent residual deformation). Numerical simulations for elastic, elastoplastic and hyperelastic contact between hemisphere and rigid plane are compared with the results of FEM to verify the accuracy of the numerical method. For non-linear elastic contact, the numerical method shows a better approximation result than linear elastic contact approximation. Finally, the numerical method is used to calculate the contact between 3D complicated rough surfaces.

2. Methods

2.1. *Linear elastic contact*

This part is the work completed by Stanley [18]. On the basis of his work, an improved calculation for elastoplastic and hyperelastic contact is proposed in this paper. In order to facilitate the understanding of the following sections, the main idea of Stanley's work is briefly introduced in this section. The readers can achieve detailed calculations by reading the original literature.

According to the research results of Westerggard [11] and Johnson [12], when a one-dimensional (or two-dimensional) sinusoidal surface and a rigid plane are in complete contact, there is a linear relationship between the sinusoidal pressure variation and the displacement. For any dimensionless pressure distribution $p^* = p / E^*$ (p is the actual pressure, E^* is the equivalent elastic modulus), p^* can can be expressed as the superposition of trigonometric series. Therefore, the expression between the deformation u and p^* for a discrete representation can be expressed by the FFT method as:

$$u\left(p^*\right) = FFT^{-1}\left(w. \times FFT\left(p^*\right)\right) \tag{1}$$

For 2D contact problems, one dimensional (1D) FFT and 1D Inverse Fast Fourier Transform (FFT^{-1}) are used, both p^* and numerical factor w are vectors. For 3D contact problems, 2D FFT and 2D FFT^{-1} are used, both p^* and w are matrices. w can be derived from the analytical formulations proposed by Westerggard and Johnson.

The final problem is to find p^* and u when two surfaces are pressed together. According to the minimization of total complementary energy, the final pressure distribution p^* and u must satisfy Eq. (2.1) in the constraint region (2.2), where f is total complementary energy, g_i is the gap between the rigid plane and undeformed surface, n is the number of discrete points and p_{target} is the average pressure. With the relationship between u and p^* in Eq. (1), the problem with two variables in Eq. (2.1) is transformed to problem with only one variable. In Stanley's work, gradient descent method is used to iteratively solve the distribution of p^* and u. The details can refer to the original literature [18].

$$\min f = \frac{1}{2}\sum_{i=1}^{n} p_i^* u_i + \sum_{i=1}^{n} p_i^* g_i \tag{2.1}$$

$$\begin{aligned} & p_i^* \geq 0, \quad 1 \leq i \leq n \\ & \frac{1}{n}\sum_{i=1}^{n} p_i^* = p_{target} \end{aligned} \tag{2.2}$$

2.2. *Non-linear elastic contact*

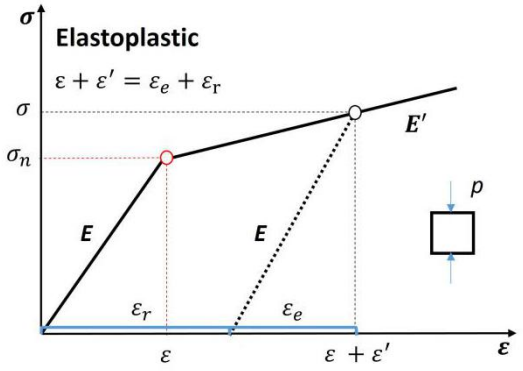

Fig. 1 Uniaxial compressive stress-strain curve with linear hardening property.

Fig. 1 shows the uniaxial compressive stress-strain curve of a material with linear hardening property. The slopes of the two linear segments are E and E' ($E > E'$). For a unit in a uniaxial compression state, when the stress is greater than the initial yield stress (σ_n), the unit will undergo plastic deformation. The corresponding strains of the two linear segments are ε and ε', respectively. The elastic strain is ε_e and plastic strain is ε_r (residual strain), then：

$$\varepsilon_r = \varepsilon + \varepsilon' - \varepsilon_e = \frac{\sigma_n}{E} + \frac{\sigma - \sigma_n}{E'} - \frac{\sigma}{E} \tag{3}$$

For units with multi-directional stresses, σ refers to the von Mises stress of the unit. It can be seen from Eq. (3) that for a unit that undergoes plastic deformation ($\sigma > \sigma_n$, $p > p_n$, p_n is the critical yield pressure), the strain solution under stress σ is equivalent to applying residual strain ε_r to the unit, and then the linear elastic contact (elastic modulus E) is used to solve the strain under stress σ. For elastoplastic contact of the entire rough surface, the solution of pressure and deformation can also be equivalent to linear elastic contact problem considering residual deformation.

The uniaxial compressive stress-strain curve of hyperelastic material such as rubber can also be simplified to a combination of two linear segments with different slopes, as shown in Fig. 2 ($E < E'$). The corresponding strains of the two linear segments are ε and ε', respectively. Similar to elastoplastic contact problem, the strain of unit is equal to the sum of the equivalent elastic strain ε_e and the equivalent residual strain ε_{er} (ε_{er} is negative), as shown in Eq. (4). For hyperelastic contact of the entire rough surface, the solution of pressure and deformation can also be equivalent to linear elastic contact problem (elastic modulus E) considering equivalent residual deformation.

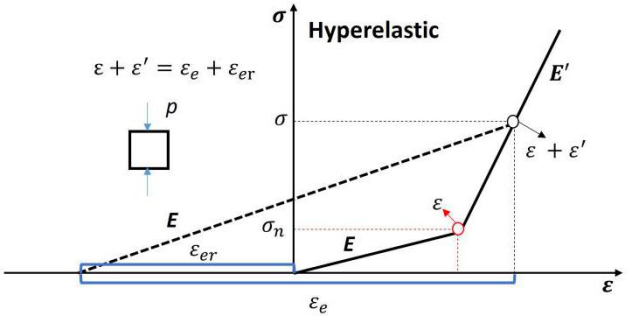

Fig. 2 Approximate uniaxial compressive stress-strain curve of hyperelastic material.

$$\varepsilon_e + \varepsilon_{er} = \varepsilon + \varepsilon' \tag{4}$$

2.3. *Algorithm*

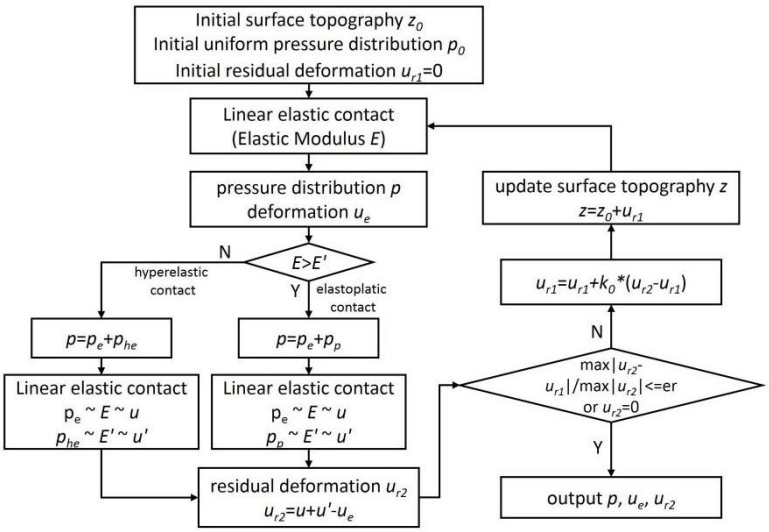

Fig. 3 Algorithm of non-linear elastic contact.

From the above analysis, it can be known that in the solution of residual deformation, if the interaction between units is ignored, all units under pressure can be simplified to a uniaxial compression state. Therefore, the solution of residual deformation is simplified. Both elastoplastic contact and hyperelastic contact problem can be equivalent to linear elastic contact considering residual deformation (or equivalent residual deformation), that is, piecewise linear elastic contact problem, so the solution algorithm is similar, as shown in Fig. 3. For the solution of elastoplastic contact (EP), first the pressure distribution p and deformation u_e can be obtained by calculating the linear elastic contact with elastic modulus E. According to the critical pressure p_n, p at each unit is decomposed into p_e and p_p, as shown in Eq. (5.1). For p_e and p_p, linear elastic contact with elastic modulus E and E' are calculated respectively. Then the corresponding deformations u and u' and residual deformation u_{r2} are calculated, as shown in Eq. (5.2). Determine whether residual deformation converges with $\max|u_{r2}- u_{r1}| / \max|u_{r2}| \le er$ (er is specification error) or $u_{r2} = 0$ (no plastic deformation in this case). If not, residual deformation u_{r1} is modified with $u_{r1}=u_{r1}+k_0\ (u_{r2}-u_{r1})$ [20], and surface topography z is updated. The process is repeated until residual deformation converges. The solution process of hyperelastic contact is similar.

$$p_e = \begin{cases} p, & 0 \le p \le p_n \\ p_n, & p > p_n \end{cases}$$

$$p_p = \begin{cases} 0, & 0 \le p \le p_n \\ p - p_n, & p > p_n \end{cases} \tag{5.1}$$

$$
\begin{aligned}
u_e &= FFT^{-1}\left(w.\times FFT\left(p^*\right)\right)\\
u &= FFT^{-1}\left(w.\times FFT\left(p_e^{\ *}\right)\right)\\
u' &= FFT^{-1}\left(\frac{E}{E'}\times w.\times FFT\left(p_p^{\ *}\right)\right)\\
u_{r2} &= u + u' - u_e
\end{aligned}
\tag{5.2}
$$

2.4. *Comparison with existing method*

Taking Jacq's work [20] as a representative of the existing numerical methods, the simplified method for elastoplastic contact proposed in this paper is compared with the existing method, as shown in Fig. 4. The difference between the two methods is mainly the way to solve the residual displacement (step ③). In the existing method, the contact pressure distribution is firstly solved by linear elastic contact calculation (step ①). Then the plastic strain distribution of bulk elements is solved according to the contact pressure distribution (step ②). Finally, the residual deformation is obtained with the plastic strain distribution (step ③). The solution of plastic strain (step ②) involves such an iterative process: The pressure stress distribution of bulk elements is solved according to the contact pressure distribution and then the von Mises stress distribution is obtained. The plastic strain distribution of bulk elements is calculated according to the linear hardening law and then the residual stress distribution is obtained. A new stress distribution of bulk elements is obtained with the superposition of the pressure stresses and the residual stresses. Then the von Mises stresses and plastic strains are solved again. The loop (P loop) is repeated until the plastic strain converges. For simplified method, the solution of residual deformation is simplified with Eq. (5-1) and Eq. (5-2) when the interaction between units is ignored.

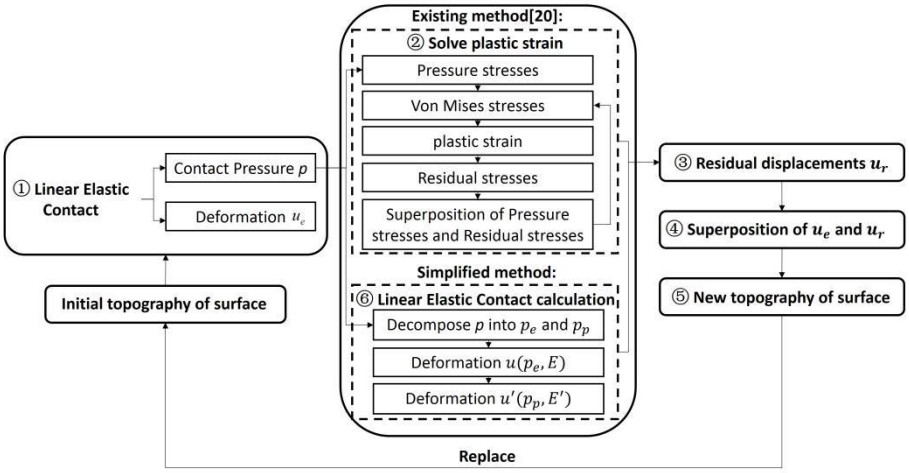

Fig. 4 Solution process comparison between Jacq's method and simplified method.

The comparison of calculation efficiency is shown in Table 1 and Table 2. For simplified method, the average loop number of step ① (E loop) is about 10, which is similar to Jacq's method. Since the iterative solution of plastic strain is not involved, it can be considered that the number of P loop is 1, and the total P loop number is only 10 for each loading step, much less than 300 in Jacq's method. In addition, according to Table 2, the effort to perform one E loop of the two

methods are similar, where m is iteration number for one E loop and N_s is the number of discrete points on the rough surface. For simplified method, the effort to perform one P loop grows as $2N_s\ln N_s$. However, the calculation of pressure stresses and residual stresses is involved in Jacq's method, so the effort to perform one P loop grows as $N_{vz}(N_s+N_{vs})\ln(N_s+N_{vs})$ and $N_{vz}^2\ N_{vs}\ln\ N_{vs}$ (N_{vz} is the number of point of the plastic volume in depth and N_{vs} is the number of points of the plastic volume per depth), which causes more calculation time. In summary, both the number of iteration and the calculation effort of each iteration of the simplified method are much smaller than Jacq's method, so the calculation efficiency can be significantly improved.

Table 1 Iteration number comparison between Jacq's method and simplified method.

	Average loop number for E loop (step ①)	Average loop number for P loop	Total P loop number for each loading step
Jacq's method	10	80-5 (step ②)	300
Simplified method	10	1 (step ⑥)	10

Table 2 Calculation effort comparison between Jacq's method and simplified method.

	One E loop (step ①)	One P loop (step ②)	
Jacq's method	$mN_s\ln N_s$	Pressure stress $N_{vz}(N_s+N_{vs})\ln(N_s+N_{vs})$	Residual stress $N_{vz}^2\ N_{vs}\ln\ N_{vs}$
Simplified method	$mN_s\ln N_s$	$2N_s\ln N_s$ (step ⑥)	

However, because the calculation of residual displacement is based on a certain simplification, the calculation accuracy will be reduced to a certain extent while the calculation efficiency is improved. For an initial average pressure distribution p_0, the pressure distribution p can be calculated according to the linear elastic contact calculation, and the actual stress state of any element is shown in Fig. 5 (a), the von Mises stress of the element is σ_{VM1}. According to Eq. (5.1), p is decomposed into p_e and p_p. The corresponding stress state of the element under p_e and p_p is shown in Fig. 5 (b) and (c) respectively. The corresponding von Mises stress is σ_{VM2} and σ_{VM3}. In fact, if the interaction between the units is considered, the pressure decomposition according to (5.1) will cause the von Mises stress error Δ e1 and residual displacement error Δ e2, as shown in Eq. (6.1) and (6.2). The value of the error is related to the actual stress state of the elements.

$$\underset{\sigma_{VM1}}{\overset{p,\,E}{\begin{bmatrix}\sigma_{x1} & \tau_{xy1} & \tau_{xz1}\\ \tau_{xy1} & \sigma_{y1} & \tau_{yz1}\\ \tau_{xz1} & \tau_{yz1} & \sigma_{z1}\end{bmatrix}}}\quad\underset{\sigma_{VM2}}{\overset{p_e,\,E}{\begin{bmatrix}\sigma_{x2} & \tau_{xy2} & \tau_{xz2}\\ \tau_{xy2} & \sigma_{y2} & \tau_{yz2}\\ \tau_{xz2} & \tau_{yz2} & \sigma_{z2}\end{bmatrix}}}\quad\underset{\sigma_{VM3}}{\overset{p_p,\,E'}{\begin{bmatrix}\sigma_{x3} & \tau_{xy3} & \tau_{xz3}\\ \tau_{xy3} & \sigma_{y3} & \tau_{yz3}\\ \tau_{xz3} & \tau_{yz3} & \sigma_{z3}\end{bmatrix}}}$$

(a) (b) (c)

Fig. 5 The stress state of element under different pressure distribution.

$$\sigma_{VM1}=\sigma_n+\Delta\sigma_{VM}=\sigma_{VM2}+\sigma_{VM3}+\Delta e1 \tag{6.1}$$

$$u_r=u(p_e)+u(p_p)-u(p)+\Delta e2 \tag{6.2}$$

3. Results and discussion

3.1. *Verification*

The contact pressure and contact area of elastic contact, elastoplastic contact and hyperelastic contact between hemisphere and rigid plane are calculated by using the numerical method in this paper. The results are compared with those of the finite element method (FEM) and Hertz analytical solutions to verify the accuracy of the algorithm. The radius of the hemisphere (R) is 0.5 mm.

3.1.1. *Linear elastic contact*

According to Hertz theory, when a load $F = 4p_0 ER^2 = p_0 E A_0$ is applied between a ball of radius R and a rigid plane, equivalent elastic modulus E^*, maximum deformation of the ball ω, contact area A, and the maximum contact pressure P_{max} can be expressed as Eq. (7) [29]:

$$\begin{aligned} E^* &= \frac{E}{1-\nu^2} \\ \omega &= \left(3p_0 E / E^*\right)^{\frac{2}{3}} R \\ A &= \pi R \omega \\ P_{\max} &= \frac{2E^*}{\pi}\left(\frac{\omega}{R}\right)^{0.5} \end{aligned} \tag{7}$$

Fig. 6 (a) shows the results of elastic contact between hemisphere (E = 210GPa, Poisson' s ratio v = 0.3) and rigid plane calculated by Hertz theory and FEM (from software ABAQUS). It can be seen that as the load increases, the dimensionless contact area $CA = A/A_0$ and the maximum contact pressure P_{max} gradually increase. When the load is small, the calculation result of Hertz theory is similar to that of FEM, which verifies the accuracy of FEM calculation within the range of small load. Moreover, the relative error of the two methods gradually increases with an increase of the load. The contact area calculated by Hertz theory is larger than that of FEM, while the maximum contact pressure result is just the opposite. According to the derivation process of Hertz theory, it can be known that the calculation result of contact area is larger than actual value, while the maximum contact pressure is smaller than actual value, which is consistent with the above results. In addition, Hertz theory is only suitable for small load and deformation. When deformation is large, calculation error is so large that Hertz theory cannot be applicable. For example, when the dimensionless load $p_0 = F/A_0E$ = 0.0003, the maximum deformation of the ball $\omega \approx 0.0042$ mm = 0.0084R and the radius of contact area $a \approx 0.0465$ mm = 0.093R, $\omega^2/a^2 \approx 0.008 \ll 1$, the calculation error is negligible, Hertz theory is applicable. When p_0 = 0.1, $\omega \approx 0.16$ mm = 0.32R and $a \approx 0.3$ mm = 0.6R, $\omega^2/a^2 \approx 0.28$, the calculation error cannot be ignored. To further verify the accuracy of FEM under large load (p_0 = 0.1), the mesh is refined from the original 17908 elements to 60282. It is found that the maximum contact pressure increases from 0.5298E to 0.5319E, and contact area increases from 0.2884A_0 to 0.2896A_0, both the relative errors are less than 0.5%. Therefore, the calculation results of FEM are considered to be accurate in the entire load range.

Since the Stanley's method (Stanley and Kato, 1997) is applicable to complete contact, w needs to be modified with $w' = k \times w$ according to FEM results. The modified results are shown in Fig. 6 (b). It can be seen that the value of k remains stable over the entire load range, about 0.135. Elastic contact with elastic modulus of 0.5E and 2E is also calculated by FEM. The results show that, no matter what the elastic modulus is, the calculation results under same p_0 are the same, indicating that the coefficient k is applicable to linear elastic contact calculation of materials with different elastic modulus. CA and P_{max} from the numerical method, and the relative errors with FEM results under different load p_0 are

calculated, as shown in Fig. 6 (b). In the entire load range, the relative error of P_{max} increases with an increase of the load, and all error values are less than 10%. While the relative error of *CA* decreases first and then increases as the load increases. For numerical simulation, *CA* is the ratio of the number of elements in the contact area (approximately circular) to the total number of elements. Compared with large load, when the load is smaller, the same error of the number of elements in the contact area will lead to a larger relative error of *CA*. In addition, the total number of elements (64 × 64 in this section) and the presence of planar area around the hemisphere (as shown in the inset of Fig. 6 (b)) also affect the relative error of contact area.

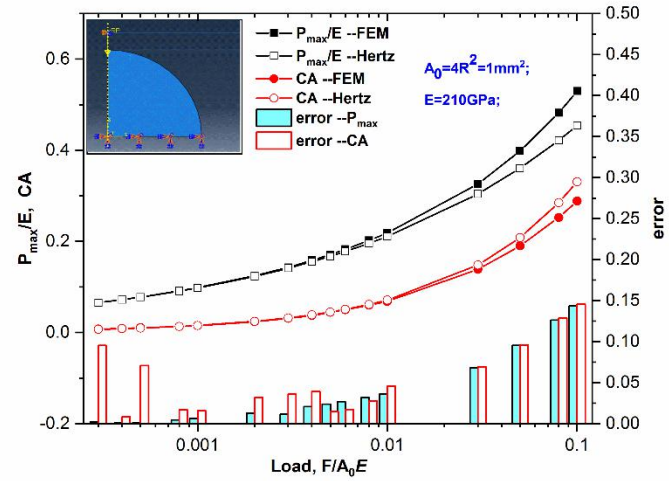

(a) Results of elastic contact by Hertz theory and FEM. 'P_{max} / E--FEM', 'P_{max} / E--Hertz', 'CA--FEM', 'CA--Hertz' represent P_{max} / E and CA calculated by FEM and Hertz theory, respectively. 'error--P_{max}' and 'error--CA' are relative error of the two methods.

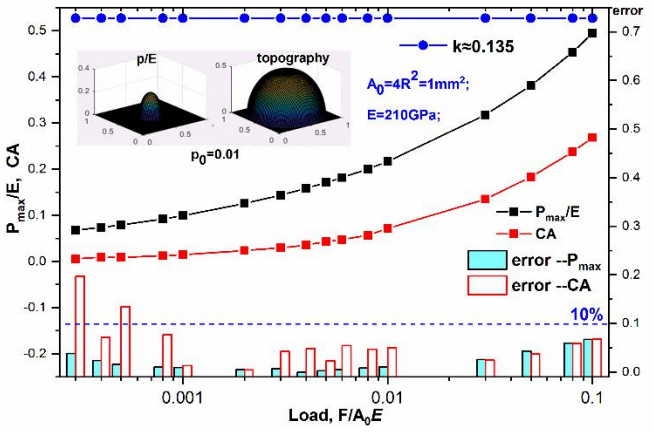

(b) Results of elastic contact by numerical method. 'k' is correction coefficient. 'error--P_{max}' and 'error--CA' are relative error of numerical method and FEM.

Fig. 6 Results of elastic contact

3.1.2. *Elastoplastic contact*

The numerical method in this paper is used to calculate the elastoplastic contact between hemisphere and rigid plane. The results are compared with linear elastic and elastoplastic calculation results of FEM, as shown in Fig. 7. The uniaxial compressive stress-strain curve of material has linear hardening property, elastic modulus E = 210 GPa, E' = 0.5E = 105 GPa, and initial yield stress σ_n = 235 MPa = 0.0011E. The yield stress σ_Y and plastic strain ε^p of the material can be expressed as Eq. (8.1) [21],

and the material property in FEM is defined accordingly. According to CEB model [29], initial yield occurs when $p > KH = K{\cdot}a{\cdot}\sigma_n = 0.6\times2.8\times235$ MPa = 394.8 MPa = 0.0019E. Therefore, Eq. (8.2) is used to define the critical pressure p_n in the numerical method. If von Mises stress is greater than yield stress σ_n in FEM, or the maximum contact pressure P_{max} is greater than critical yield pressure p_n in the numerical method, the material will yield.

$$\sigma_Y = \sigma_n + \frac{E'}{1 - E'/E}\varepsilon^p \tag{8.1}$$

$$p_n = KH = 1.68\sigma_n \tag{8.2}$$

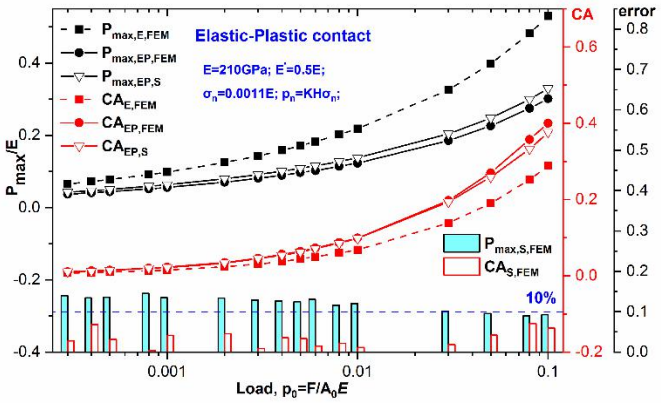

Fig. 7 Results of elastoplastic contact by numerical method. '$P_{max,E,FEM}$', '$P_{max,EP,FEM}$', '$P_{max,EP,S}$' represent P_{max} / E of elastic contact by FEM, elastoplastic contact by FEM and elastoplastic contact by numerical method. The representation of CA is similar. '$P_{max,S,FEM}$', 'CA$_{S,FEM}$' are relative error of elastoplastic contact of numerical method and FEM.

It can be seen from Fig. 7 that if plastic deformation is considered, the maximum contact pressure P_{max} decreases and contact area CA increases under the same load. Compared with linear elastic contact, the elastoplastic contact results of P_{max} and CA calculated by numerical method are closer to those of FEM results. Yield occurs over the entire load range, and plastic deformation area increases with increasing load. The error of elastoplastic contact by numerical method comes from the calculation of linear elastic contact and the solution of residual deformation. When load p_0 is in the range of 0.0003~0.1, the relative error of contact area is small, and the relative error of maximum contact pressure is less than 15%.

In the above numerical calculation for elastoplastic contact, the total number of elements is 64 × 64 = 4096 and specification error er (as shown in Fig. 3) is 0.03. In order to analyze the influence of the number of grids and the value of er on the calculation results, the calculation time and calculation error of P_{max} under different er (0.01, 0.03, 0.05, 0.1) and different grid number (16× 16, 32 × 32, 64 × 64, 128 × 128) are analyzed, as shown in Fig. 8. It can be seen from Fig. 8 (a) that within the load range, the calculation time is within 1-9 min and the calculation error is in the range of 9.5-14.5 %, both decreasing as the load increases. At the same grid number and the same load, the calculation time slightly decreases and the calculation error slightly increases as er increases. For the influence of grid number, as shown in Fig. 8 (b), at the same er and the same load, the calculation time grows as the grid number, and the time span is large. When the grid number is 16×16, the calculation time does not exceed 1min; When the grid number is 32 × 32, the calculation time is 0-2.5min; When the grid

number is 64 × 64, the calculation time is 2-8 min; When the grid number is 128 × 128, the calculation time is 8-47 min. However, except for the larger calculation error with grid number 16×16, the calculation error corresponding to the other three sets of grid number are almost the same. Therefore, considering the calculation time and calculation error, grid number with 32 × 32 or 64 × 64 is a better choice.

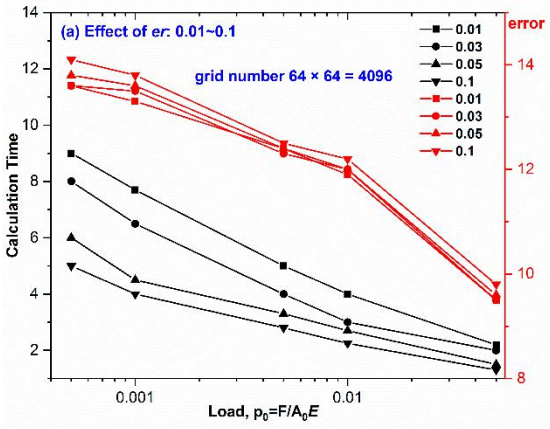

(a) Calculation results under different *er*.

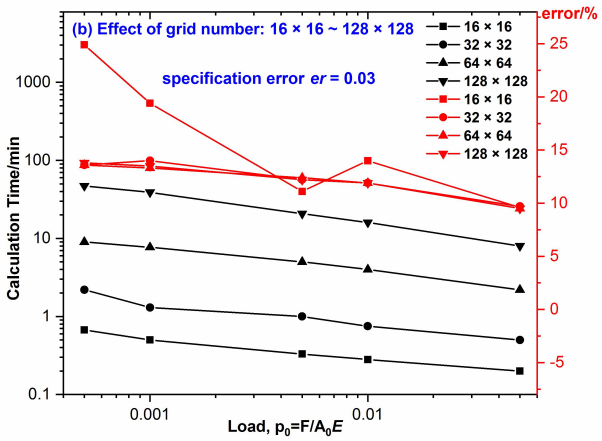

(b) Calculation results under different grid number.

Fig. 8 Calculation results under different *er* and different grid number.

3.1.3. *Hyperelastic contact*

The contact behavior between hyperelastic hemisphere and rigid plane is calculated. In FEM, the constitutive model of rubber needs to be defined according to the compressive stress-strain curve of material, as shown in Fig. 9 (a). It can be seen that among the five fitted constitutive models, the Ogden[3] model has the best fitting result, so it is selected for defining material property in FEM. For numerical simulation, the original stress-strain curve needs to be simplified to a combination of two linear segments. As shown in Fig. 9 (b), there are three simplified results: FC1, FC2 and FC3. The parameters of each fitted curve are as shown in the table. It shows that elastic modulus E and E' have four kinds of values, and critical stress has three values for the three results.

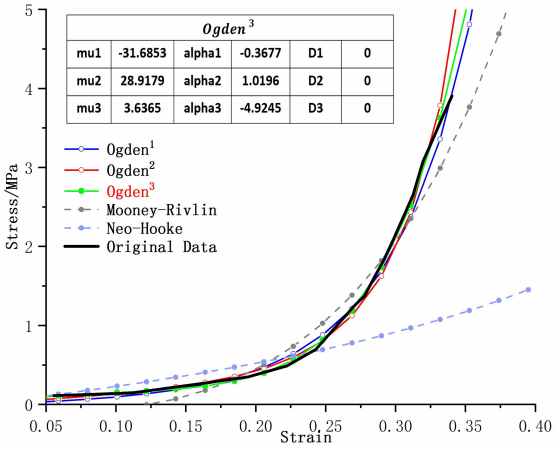

(a) Constitutive model fitting of rubber for FEM.

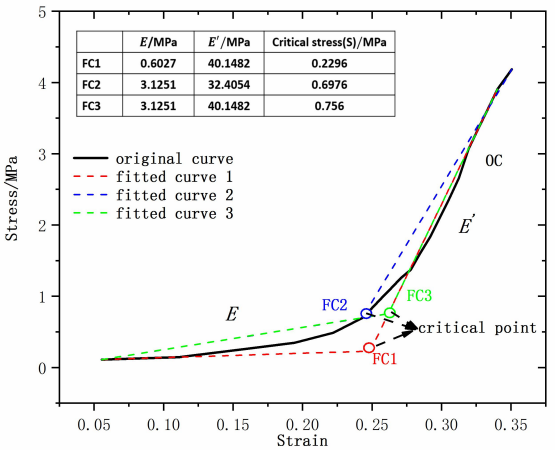

(b) Simplification of stress-strain curve for numerical method.

Fig.9 Fitting results of compressive stress-strain curve of material.

The hyperelastic contact calculation under different load (0.001 ~ 50 N) is performed by FEM. According to Fig. 9 (b), two elastic moduli E_1 = 3.1251 MPa and E_2 = 32.4054 MPa are selected as elastic modulus of linear elastic contact respectively to approximate the hyperelastic contact (ν = 0.49), as shown in Fig. 10. It can be seen that the approximation results can be artificially divided into three regions. When the load is small, linear elastic contact result with lower elastic modulus E_1 is closer to hyperelastic contact result (area A). When the load is large, linear elastic contact calculation with higher elastic modulus E_2 has a better approximation result (area C). Between the two regions (area B), the approximation errors of linear elastic contact with both two elastic moduli are relatively large. For approximation by linear elastic contact calculation, the selection of elastic modulus E and the approximation result are related to the load and material property, which is unclear now, especially for complicated rough surface. Therefore, the numerical method in this paper is used to approximate the hyperelastic contact calculation.

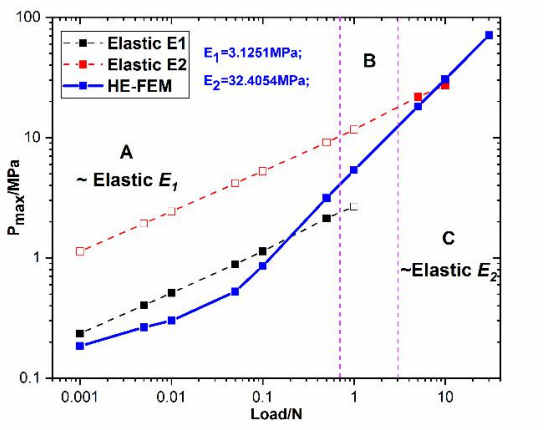

(a) Variation in the maximum contact pressure P_{max} with load.

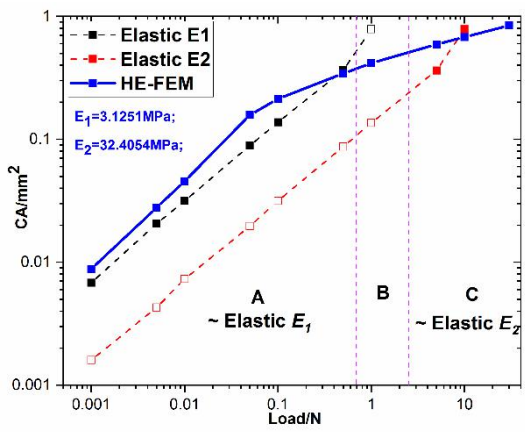

(b) Variation in dimensionless contact area CA with load.

Fig. 10 Results of hyperelastic contact and approximation by linear elastic contact calculation in FEM. 'Elastic E1', 'Elastic E2' represent the linear elastic contact results in FEM with elastic modulus E_1 and E_2, respectively. 'HE-FEM' represents the results of hyperelastic contact calculation in FEM.

According to Fig. 10, the load values of 0.01 N, 1 N and 5 N are selected in each area A, B and C. For the three fitted curves FC1, FC2 and FC3, non-linear elastic contact calculation by numerical method is performed under the selected three loads (critical pressure p_n is calculated according to Eq. (8.2)). The results of pressure distribution along the radius of contact area are shown in Fig. 11. When the load is 0.01 N (Fig. 11 (a)), the maximum contact pressure of the three fitted curves calculated by numerical method are all smaller than the corresponding critical pressures, therefore they are all in the state of linear elastic contact calculation. Curve ② corresponds to linear elastic contact approximation with elastic modulus of 0.6027 MPa, curve ③, ④ and ⑤ are equivalent to linear elastic contact approximation with elastic modulus of 3.1251 MPa, and curve ⑥ corresponds to linear elastic contact approximation with elastic modulus of 32.4054 MPa. It can be seen that under a small load, linear elastic contact with lower elastic modulus E_1 and non-linear elastic contact of the three fitted curves have better approximation results. When the load is 1 N (Fig. 11 (b)) or 5 N (Fig. 11 (c)), numerical calculations of the three fitted curves are all in the state of non-linear elastic contact calculation. When the load is 1 N, compared with the large approximation error of linear elastic contact with either lower elastic modulus E_1 or higher elastic modulus E_2, the three non-linear elastic contact calculations have better approximation results. When load is 5 N (5 N is too large for linear elastic contact with elastic

modulus E_1 to converge in FEM, so it is not calculated), the two non-linear elastic contacts of fitted curves FC2 and FC3 fit better. In conclusion, compared with approximation by linear elastic contact with a specific elastic modulus, the advantage of non-linear elastic contact approximation is that the calculation results of hyperelastic contact can be better fitted within the load range in this paper. For this example, considering calculation efficiency and approximation results, FC3 is the best of the three fitted curves. The calculation error of this numerical method mainly comes from the fitting results of stress-strain curve, linear elastic contact calculation, and the solution of equivalent residual deformation. In theory, in order to better fit the calculation results of hyperelastic contact, the original stress-strain curve can be simplified to a combination of multiple linear segments with a shape closer to the original curve.

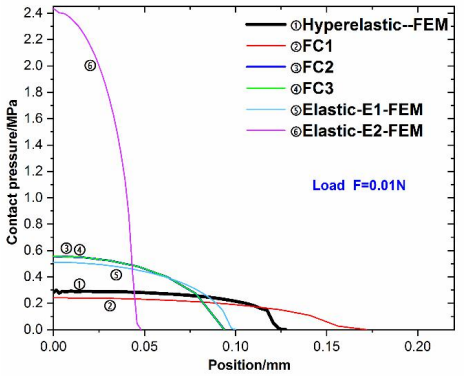

(a) Pressure distribution under load of 0.01 N.

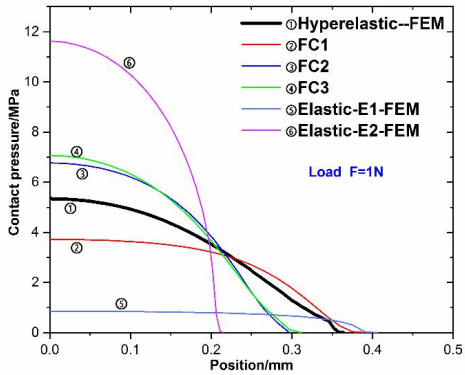

(b) Pressure distribution under load of 1 N.

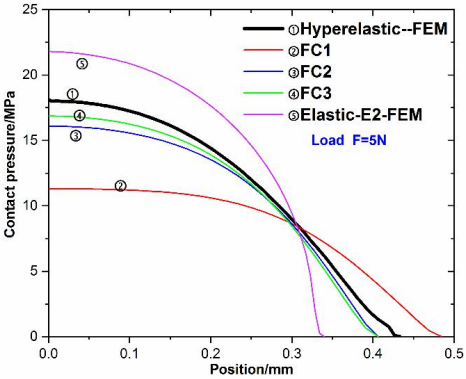

(c) Pressure distribution under load of 5 N.

Fig. 11 Pressure distribution along the radius of contact area. 'Hyperelastic--FEM' represents the result of hyperelastic contact calculation in FEM. 'FC1', 'FC2', 'FC3' represent the results of non-linear elastic contact calculation with fitted

curves FC1, FC2 and FC3 in numerical method, respectively. 'Elastic-E1-FEM' and 'Elastic-E2-FEM' represent the results of elastic contact calculation with elastic modulus of E_1 and E_2 in FEM, respectively.

3.2. *Contact calculation of 3D rough surfaces*

3.2.1. *Machined rough surface*

For the contact between the machined rough surface and the rigid plane (Fig. 12 (a)), the typical form of the cross section of the leak path formed at the interface contact is determined to be a triangle with $\alpha \approx 4°$ [30]. As shown in Fig. 12 (b), the height of initial undeformed cross section of leak path is h_0. Under the applied load $F = p_0 E_0 2x_0 l_0$, the contact area between rough surface and the rigid plane is A_c. The cross section of leak path is approximately reduced in proportion, and the deformed height is reduced to h. Therefore, the relationship between h and A_c can be expressed as Eq. (9), where CA is dimensionless contact area. Take the laminar flow of an incompressible fluid as an example, the viscosity of the fluid is η. When the fluid pressure difference across the leak path is Δp, the leak rate of a single deformed leak path can be calculated as Eq. (10) [31]. q_V is the volume flow rate.

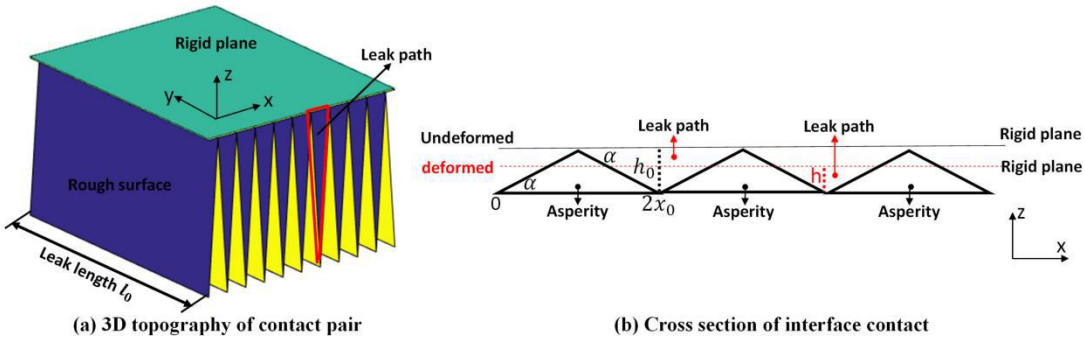

(a) 3D topography of contact pair (b) Cross section of interface contact

Fig. 12 The contact between the machined rough surface and the rigid plane.

$$h = h_0(1 - A_c / 2x_0 l_0) = h_0(1 - CA) \tag{9}$$

$$dq_V = \frac{z^3 \Delta p}{12\eta l_0} dx = \frac{x^3 \tan^3 \alpha \Delta p}{12\eta l_0} dx \tag{10.1}$$

$$q_V = 2\int_0^{\frac{h}{\tan\alpha}} \frac{x^3 \tan^3 \alpha \Delta p}{12\eta l_0} dx = \frac{h^4 \Delta p}{24\eta l_0 \tan\alpha} \tag{10.2}$$

It can be seen from Eq. (9) and (10) that in order to obtain the volume flow rate, the contact area A_c or dimensionless contact area CA needs to be solved according to the applied load. Therefore, the numerical method in this paper is used to calculate linear elastic, elastoplastic and hyperelastic contact between machined rough surface (the relevant parameters are shown in Table 3) and rigid plane. In this example, the height of initial undeformed cross section of leak path h_0 is 2μm, the total number of elements is 64 × 64 = 4096 and specification error er is 0.03. The calculation results are shown in Fig. 14. It can be seen that as the load increases, the contact area gradually increases. For elastoplastic contact, under the same load, the contact area is larger than that of elastic contact and increases with the decrease of E'. For hyperelastic contact, compared with elastic contact, the contact area is reduced and increases with the decrease of E'.

Table 3 Relevant parameters of different materials.

	E	E'	v	Critical pressure (p_n)
Elastic	E_0	——	0.3	——
Elastoplastic(EP)	E_0	0.5 E_0	0.3	0.002 E_0
Elastoplastic(EP)	E_0	0.8 E_0	0.3	0.002 E_0
Hyperelastic(HE)	E_0	10 E_0	0.49	0.4 E_0
Hyperelastic(HE)	E_0	5E_0	0.49	0.4 E_0

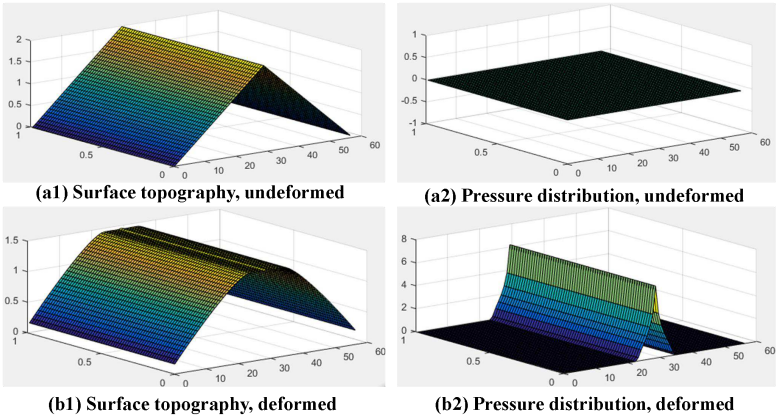

Fig. 13 Surface topography and pressure distribution of undeformed and deformed condition. p_0=0.5. Take elastic contact calculation as an expamle, the results of elastoplastic and hyperelastic contact are similar.

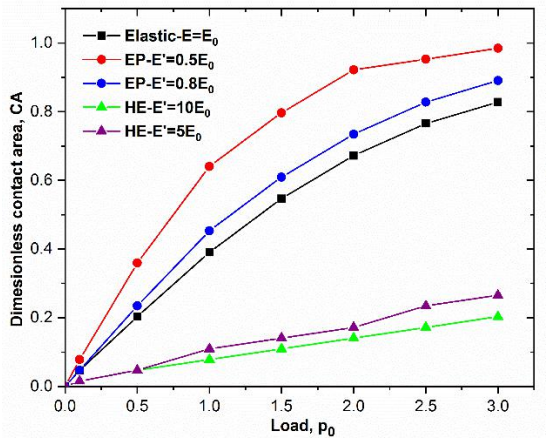

Fig. 14 Dimensionless contact area *CA* with different materials.

It can be seen from Eq. (10) that q_V is proportional to h^4 when Δp, l_0 and η remain constant, so h^4 is calculated to compare the relative value of the leakage rate, as shown in Fig. 15. Contrary to the calculation result of the contact area, q_V is reduced and the difference of q_V with different materials increases as the load increases. For elastoplastic contact, under the same load, the flow rate is less than that of elastic contact and decreases with the decrease of E'. For hyperelastic contact, compared with elastic contact, the flow rate increases and decreases with the decrease of E'.

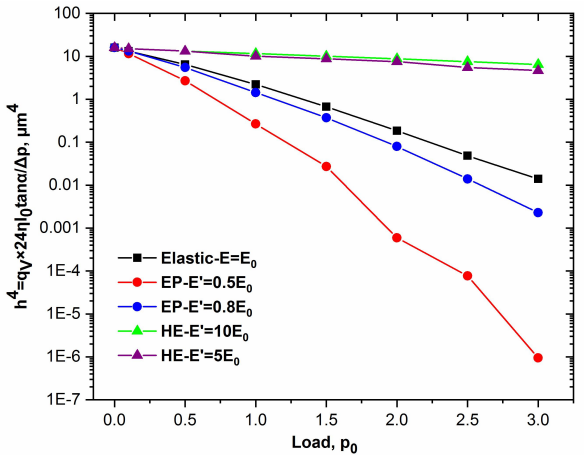

Fig. 15 Volume flow rate with different materials.

3.2.2. *Random rough surface*

For an anisotropic complicated rough surface, if the surface topography is known, the leakage channel can be determined by lattice leakage model [32] and the leakage rate can be calculated by Eq. (10.1). Topography of undeformed rough surface is shown in Fig. 16, where the length and width of the rough surface are Δx and Δy, respectively. The undeformed profile is given in Eq. (11), the unit of z is μm.

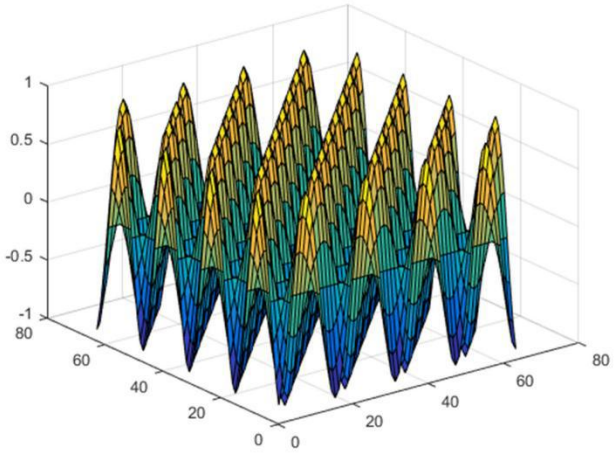

Fig. 16 The topography of undeformed rough surface.

$$z = \cos(\frac{\pi x}{8})\cos(\frac{\pi y}{8}) \tag{11}$$

The contact area and leakage rate are calculated and the results are shown in Fig. 17 and Fig. 18. In this example, the total number of elements is 64 × 64 = 4096 and specification error *er* is 0.03. Similar to the calculation results in Section 3.2.1, for the same material, the contact area increases and the leakage rate decreases as the load increases. The influence of different materials on the calculation results is also the same as the results of Section 3.2.1. However, for elastoplastic contact in this example, when the contact area is greater than a certain value, there is no through leakage channel, so the leakage rate is reduced to 0.

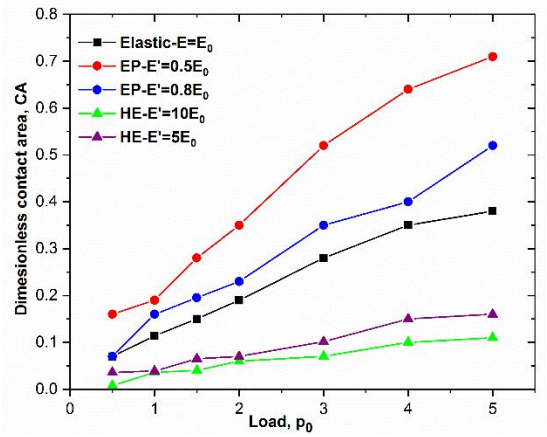

Fig.17 Dimensionless contact area *CA* with different materials.

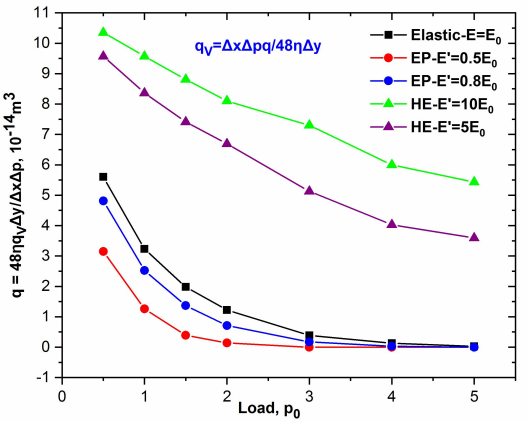

Fig. 18 Volume flow rate with different materials.

Take the calculation results of elastoplastic contact with $E' = 0.5\ E$ as an example, as shown in Fig. 19. In the plan view of the leak channel (b1-b3), blue indicates the contact field, green indicates the through leak channel, and white indicates the leak channel with no fluid passing through. When the applied load p_0 is in the range of 0.5~2, the dimensionless contact area is less than 0.35 and there is a through leakage channel. When p_0 is greater than 3, the contact area is too large to form a through leakage channel, so the leakage rate is 0.

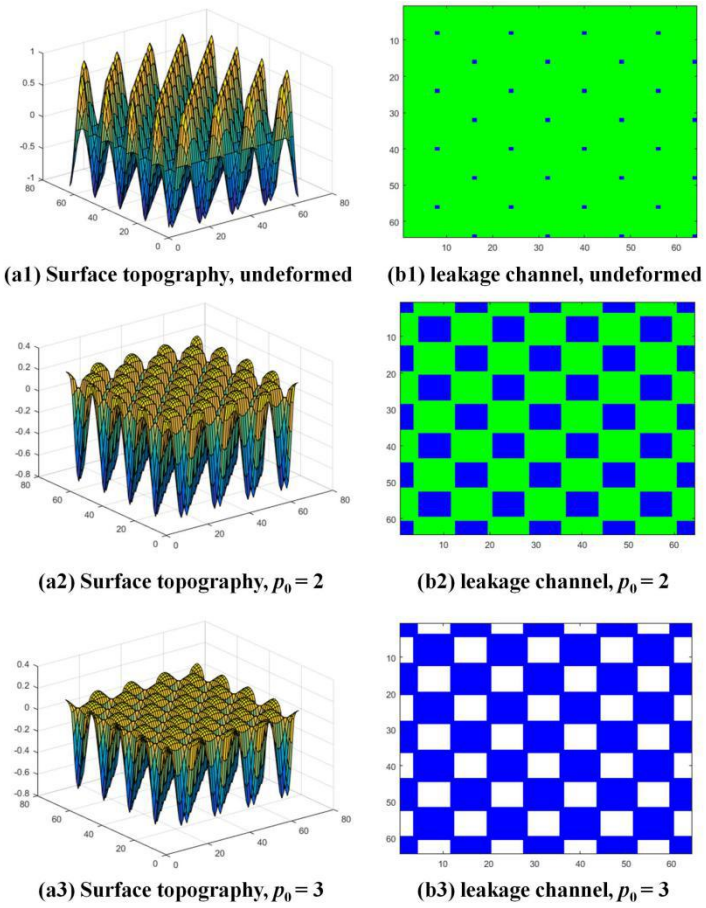

Fig. 19 Surface contact state evolution of elastoplastic contact with $E' = 0.5\ E$.

4. Conclusion

Based on FFT, a numerical method suitable for elastoplastic and hyperelastic frictionless contact is proposed in this paper, which can be used to solve 2D and 3D contact problems. The non-linear elastic contact problem is transformed to linear elastic contact problem considering residual deformation (equivalent residual deformation) and the solution of residual deformation (equivalent residual deformation) is simplified. For elastoplastic contact, the calculation efficiency is improved at the expense of certain calculation accuracy in the proposed method. For hyperelastic contact, the proposed method reduces the dependence of the approximation result on load in linear elastic approximation. Therefore, there is no need to select elastic modulus according to load, material property and other factors as in the linear elastic contact approximation. In some engineering applications, contact calculation between complicated rough surfaces and fluid-solid coupling are involved. Most of the processing methods are to use linear elastic contact result as the approximation result to reduce the calculation time, which needs to be improved in calculation accuracy. The proposed method provides a compromise solution for such problems, so it is expected to have certain application value in engineering applications.

The method proposed in this paper is a simplified method to solve the non-linear elastic contact problem. Therefore, the improvement of calculation accuracy and residual deformation solution are

expected to be further solved. For linear elastic calculation process in the algorithm, the relaxation factor k_0 related to residual deformation in the algorithm also affect the convergence and calculation efficiency of the algorithm. Therefore, it is necessary to study further to improve the calculation efficiency. In order to better fit the calculation results of hyperelastic contact, the original stress-strain curve can be simplified to a combination of multiple linear segments and the approximation results can be further discussed.

Nomenclature

F = load, N

f = total complementary energy

g_i = the gap between the rigid plane and undeformed surface, n is the number of discrete points

n = the number of discrete points

er = specification error

m = iteration number for one E loop

N_s = the number of discrete points on the rough surface

N_{vz} = the number of point of the plastic volume in depth

N_{vs} = the number of points of the plastic volume per depth

σ_{VM1} = von Mises stress of element at p

σ_{VM2} = von Mises stress of element at p_e

σ_{VM3} = von Mises stress of element at p_p

Δ e1 = von Mises stress error

Δ e2 = residual displacement error

p, p_n = contact pressure, critical pressure, MPa

p_{max} = maximum contact pressure, MPa

p_0, p^*, p_e^*, p_p^* = dimensionless contact pressure

E_0, E, E', E_1, E_2 = elastic modulus

v = Poisson' s ratio

E^* = equivalent elastic modulus

u, u' = displacement, mm

u_e, u_r = elastic dispalcement, residual displacement, mm

σ, σ_n = stress, initial yield stress, MPa

ε, ε' = strain

ε_e, ε_r = elastic strain, residual strain

z_0, z = surface topography

A_0, A, A_c = contact area

CA = dimensionless contact area

w = coefficient in FFT

N = number of 1D elements

k = correction coefficient in numerical method

k_0 = relaxation factor

R = radius of hemisphere, mm

ω = maximum deformation, mm

a = radius of contact area, mm

α = angle of the cross section of the leak path

h_0 = the height of initial undeformed cross section of leak path

h = the height of deformed cross section of leak path

l_0 = leak length

x_0 = base length of initial undeformed cross section of leak path

η = the viscosity of fluid

Δp = the fluid pressure difference across the leak path

q_V = the volume flow rate

Δ x = the length of rough surface

Δ y = the width of rough surface

q = leakage rate parameter, $q = 48\eta q_V \Delta y / \Delta x \Delta p$

Declaration

Availability of data and materials: All of the work and samples are original and repeatable, the paper contains no material previously published or written by another person except where due reference is made in the paper itself.

Competing interests: The authors declare that they have no known competing financial interests or personal relationships that could have appeared to influence the work reported in this paper.

Funding: The work described in this paper has been supported by the National Key R&D Program of China (Grant No. 2019YFB1505301), the National Natural Science Foundation of China (Grant No. U1937602), the Aeronautical Science Foundation of China (Grant No. 201907058001) and the Open Research Fund of State Key Laboratory of Smart Manufacturing for Special Vehicles and Transmission System (Grant No. GZ2019KF013).

Authors' contributions:

Fei Guo:

The proposal of new methods (2. Methods.).

The calculation of linear elastic contact by the new numerical method. (3.1.1. Linear elastic contact.).

The calculation of elastoplastic contact by the new numerical method. (3.1.2. Elastoplastic contact.).

Analysis of results and writing of paper.

Fan Wu:

Programming of the elastic contact model proposed by Stanley. (2. Methods.).

The calculation of hyperelastic contact by the new numerical method and FEM results. (3.1.3 Hyperelastic contact).

Analysis of results and writing of 3.1.3.

Xinyong Li:

The calculation of linear elastic contact, elastoplastic contact by FEM. (3.1.1-3.1.3.).

Yijie Huang:

Programming of lattice leakage model and solution random rough surface contact. (3.2.2. Random rough surface.)

Zhuo Wang:

Solution of machined rough surface contact. (3.2.1. Machined rough surface.)

Acknowledgements:

The author is indebted to Dr. Chong Xiang for the guidance on the programming process.

References

[1] Guo F., Jia X H, Suo S F, et al. (2013) A mixed lubrication model of a rotary lip seal using flow factors. Tribology International. 57: 195–201.

[2] Li S., Niu W T, Li H T, et al. (2015) Numerical analysis of leakage of elastomeric seals for reciprocating circular motion. Tribology International. 83: 21-32.

[3] Sun J J, Ma C B, Lu J H, et al. (2018) A leakage channel model for sealing interface of mechanical face seals based on percolation theory. Tribology International. 118: 108-119.

[4] Xiang C, Guo F, Jia X H, et al. (2019) Thermo-elastohydrodynamic mixed-lubrication model for reciprocating rod seals. Tribology International. 140: 105894.

[5] Xiang C, Guo F, Liu X, et al. (2020) Numerical algorithm for fluid–solid coupling in reciprocating rod seals. Tribology International. 143: 106078.

[6] Greenwood J A, Williamson J B. (1966) Contact of Nominally Flat Surfaces. Proceedings of the Royal Society of London. Series.A. Mathematical and physical sciences. 295(1442): 300-319.

[7] Xiao H F, Sun Y Y. (2019) On the normal contact stiffness and contact resonance frequency of rough surface contact based on asperity micro-contact statistical models. European Journal of Mechanics A-Solid. 75: 450-460.

[8] Xu Y, Jackson R L. (2017) Statistical models of nearly complete elastic rough surface contact-comparison with numerical solutions. Tribology International. 105: 274-291.

[9] Morag Y, Etsion I. (2007) Resolving the contradiction of asperities plastic to elastic mode transition in current contact models of fractal rough surfaces. Wear. 262(5-6): 624-629.

[10] Miao X M, Huang X D. (2014) A complete contact model of a fractal rough surface. Wear. 309(1-2): 146-151.

[11] Westerggard H M. (1939) Bearing pressures and cracks. Journal of Applied Mechanics-Transactions of the ASME. 6: 49-53.

[12] Johnson K L, Greenwood J A, Higginson J G. (1985) The contact of elastic regular wavy surfaces. International Jouranal of Mechanical Sciences. 27(6): 383-396.

[13] Zhu H B, Zhao Y T, He Z F, et al. (2018) An elastic-plastic contact model for line contact structures. Science China-Physics Mechanics & Astronomy. 61(5): 054611.

[14] Kogut L., Etsion I. (2002) Elastic-plastic contact analysis of a sphere and a rigid flat. International Journal of Applied Mechanics. 69(5): 657-662.

[15] Bryant M J, Evans H P, Snidle R W. (2012) Plastic deformation in rough surface line contacts — a finite element study. Tribology International. 46(1): 269-278.

[16] Wei D H, Zhai C P, Hanaor D, et al. (2020) Contact behaviour of simulated rough spheres generated with spherical harmonics. International Journal of Solids and Structures. 193: 54-68.

[17] Polonsky I A, Keer L M. (1999) A numerical method for solving rough contact problems based on the multi-level multi-summation and conjugate gradient techniques. Wear. 231(2): 206-219.

[18] Stanley H M, Kato T. (1997) An FFT-based method for rough surface contact. Journal of Tribology-Transactions of the ASME. 119(3): 481-485.

[19] Wang W Z, Wang H, Liu Y C, et al. (2003) A comparative study of the methods for calculation of surface elastic deformation. Proceedings of the Institution of Mechanical Engineers Part J-Journal of Engineering Tribology. 217(2): 145-154.

[20] Jacq C, Ne´lias D, Lormand G, et al. (2002) Development of a three-dimensional semi-analytical elastic-plastic contact code. Journal of Tribology-Transactions of the ASME. 124(4), 653-667.

[21] Wang F, Keer L M. (2005) Numerical simulation for three dimensional elastic-plastic contact with hardening behavior. Journal of Tribology-Transactions of the ASME. 127(3): 494-502.

[22] Chen W W, Liu S B, Wang Q J. (2005) Fast Fourier Transform based numerical methods for elasto-plastic contacts of nominally flat surfaces. International Journal of Applied Mechanics. 75(1): 011022.

[23] Kossa A, Szabó L. (2010) Numerical implementation of a novel accurate stress integration scheme of the von

Mises elastoplasticity model with combined linear hardening. Finite Elements in Analysis and Design. 46(5): 391-400.

[24] Majeed M A, Yigit A S, Christoforou A P. (2012) Elastoplastic contact/impact of rigidly supported composites. Composites Part B-Engineering. 43(3): 1244-1251.

[25] Fulleringer B, Nelias D. (2010) On the Tangential Displacement of a Surface Point Due to a Cuboid of Uniform Plastic Strain in a Half-Space. International Journal of Applied Mechanics. 77(2): 021014.

[26] Kucharski S, Starzyński G. (2019) Contact of Rough Surfaces under Normal and Tangential Loading. Wear. 440: 203075.

[27] Johansson L. (1993) Model and Numerical Algorithm for Sliding Contact between Two Elastic Half-Planes with Frictional Heat Generation and Wear. Wear. 160(1): 77–93.

[28] Wen Q F, Liu Y, Huang W F, et al. (2013) The Effect of Surface Roughness on Thermal-Elasto-Hydrodynamic Model of Contact Mechanical Seals. Science China-Physics Mechanics & Astronomy. 56(10): 1920–1929.

[29] Chang W R, Etsion I. (1987) An Elastic-Plastic Model for the Contact of Rough Surfaces. Journal of Tribology-Transactions of the ASME. 109(2): 257–263.

[30] Roth A. (1972) The interface-contact vaccum sealing processes. Journal of Vaccum Science & Technology A. 9(1): 14-23.

[31] Gu B Q, Li X H, Tian Z. (2004) Static seal design technology. China.

[32] Shi J C, Liu J H, Yang Z M, et al. (2016) On the Multi-scale Contact Behavior of Metal Rough Surface Based on Deterministic Model. Chinese Journal of Mechanical Engineering. 53(3): 111-20.

Figures

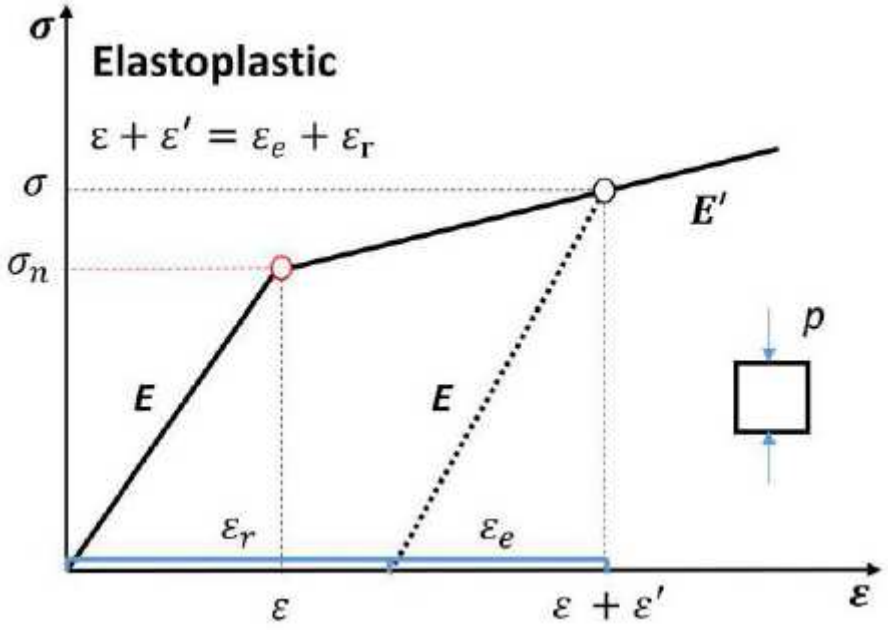

Figure 1

Uniaxial compressive stress-strain curve with linear hardening property.

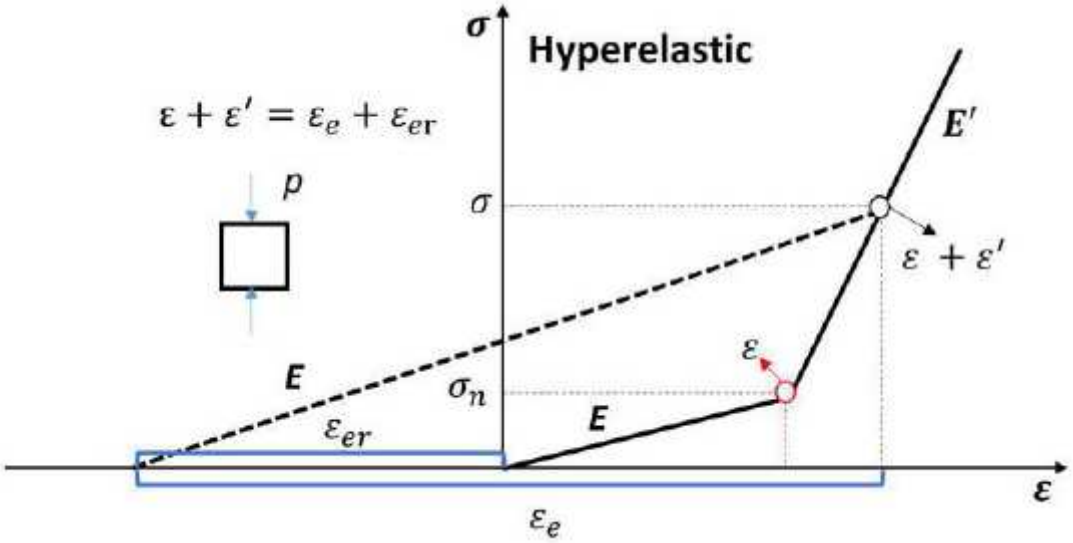

Figure 2

Approximate uniaxial compressive stress-strain curve of hyperelastic material.

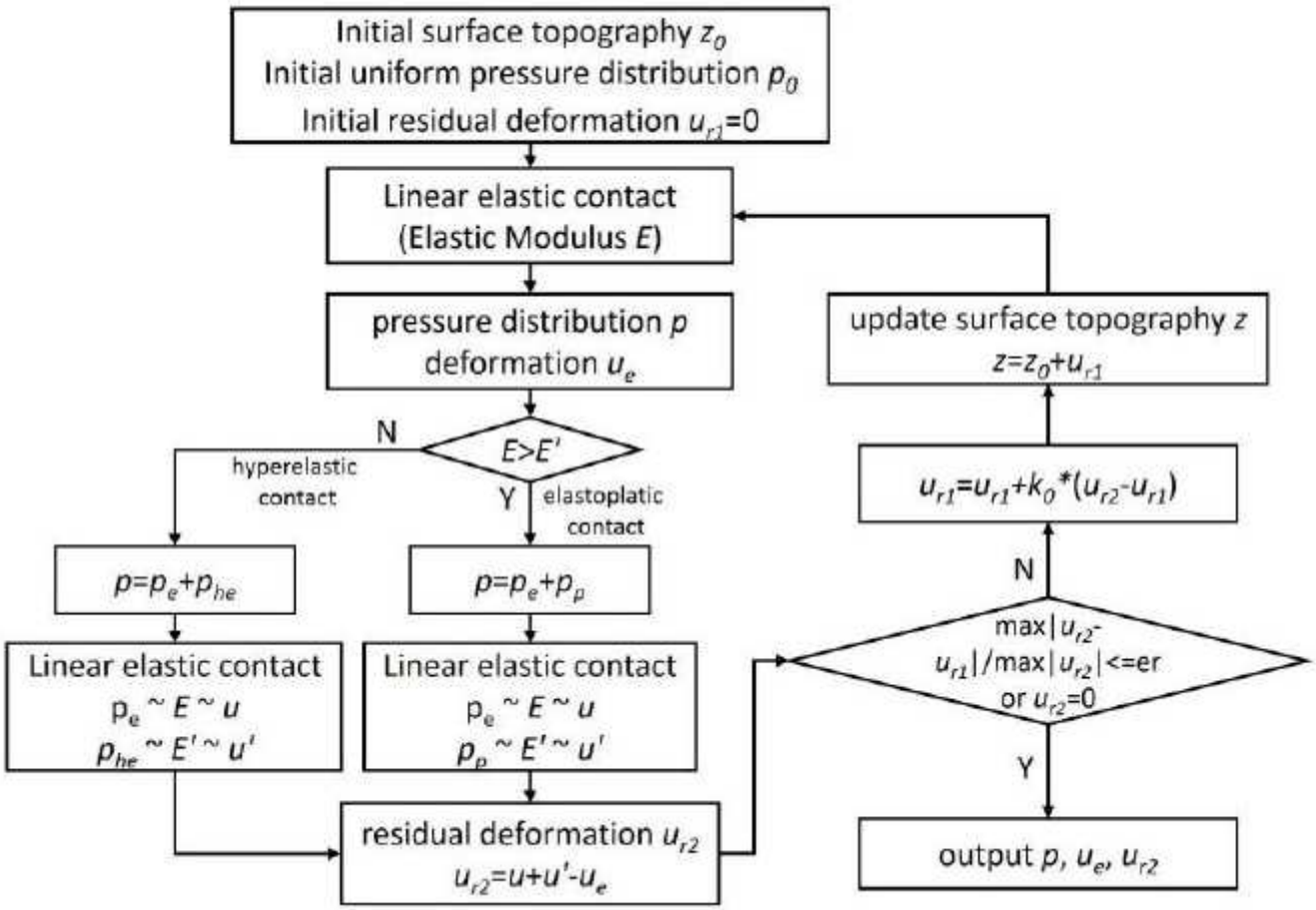

Figure 3

Algorithm of non-linear elastic contact.

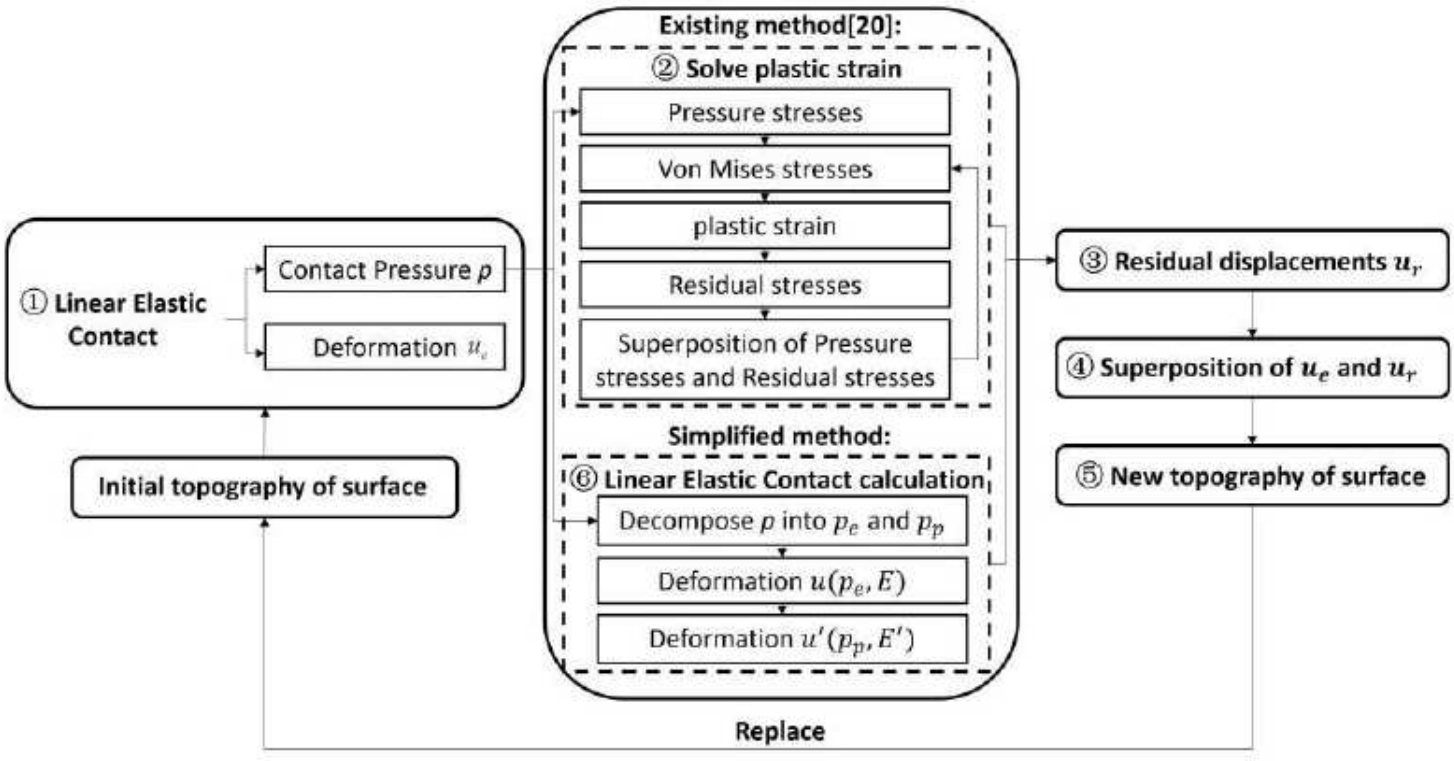

Figure 4

Solution process comparison between Jacq's method and simplified method.

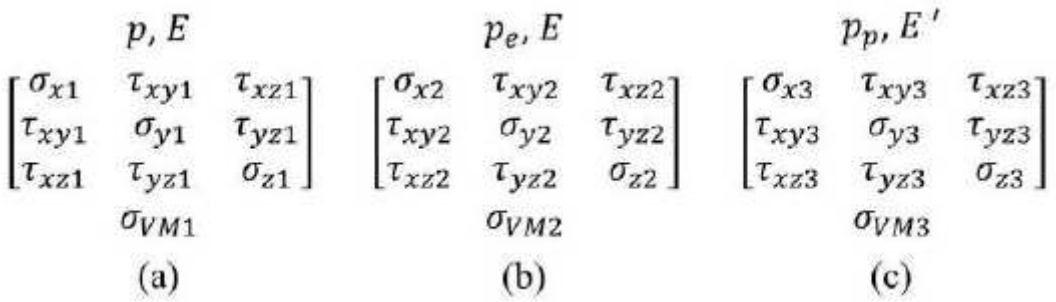

Figure 5

The stress state of element under different pressure distribution.

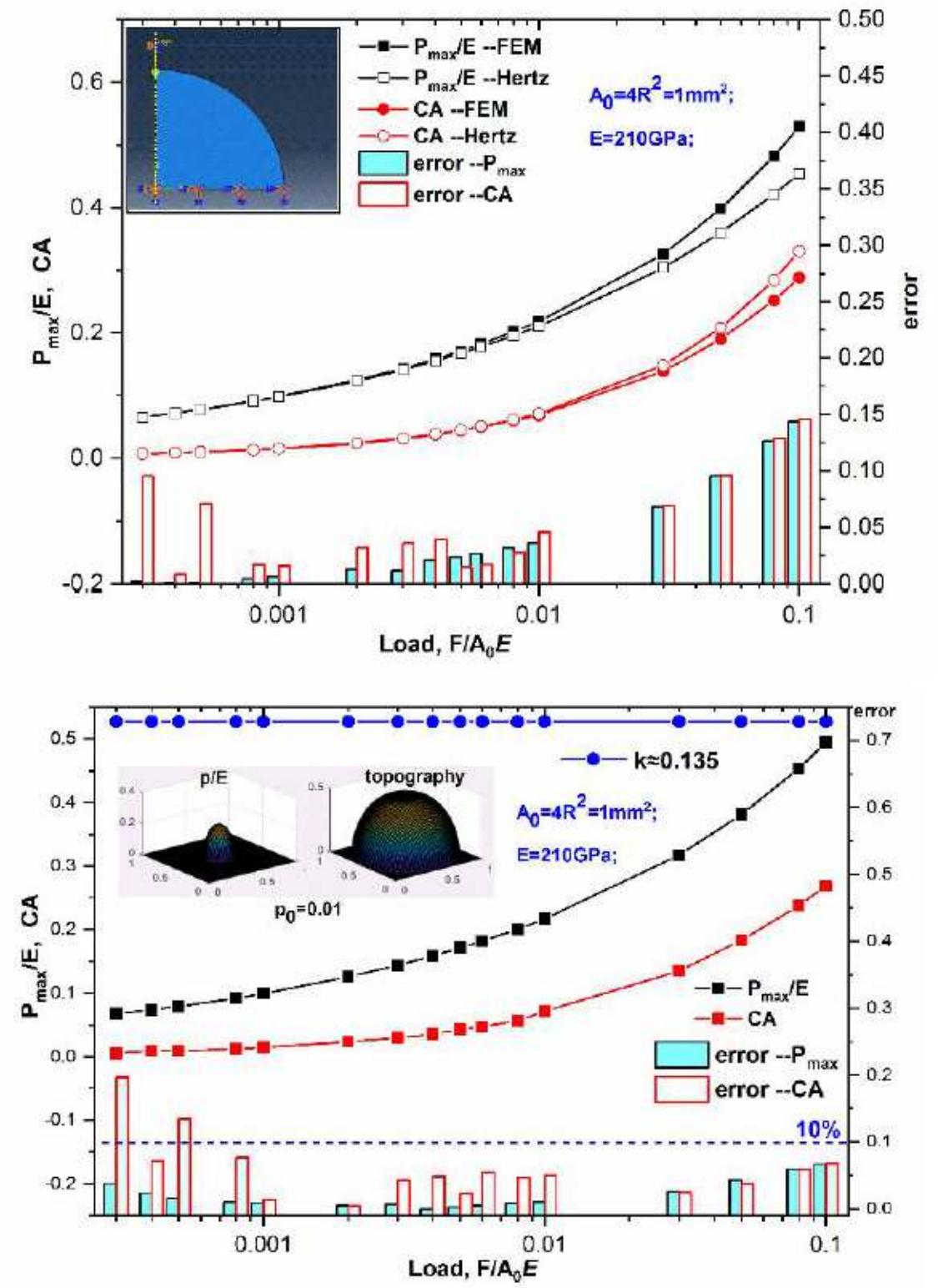

Figure 6

Results of elastic contact (a) Results of elastic contact by Hertz theory and FEM. 'Pmax / E–FEM', 'Pmax / E–Hertz', 'CA–FEM', 'CA–Hertz' represent Pmax / E and CA calculated by FEM and Hertz theory, respectively. 'error–Pmax' and 'error–CA' are relative error of the two methods. (b) Results of elastic contact by numerical method. 'k' is correction coefficient. 'error–Pmax' and 'error–CA' are relative error of numerical method and FEM.

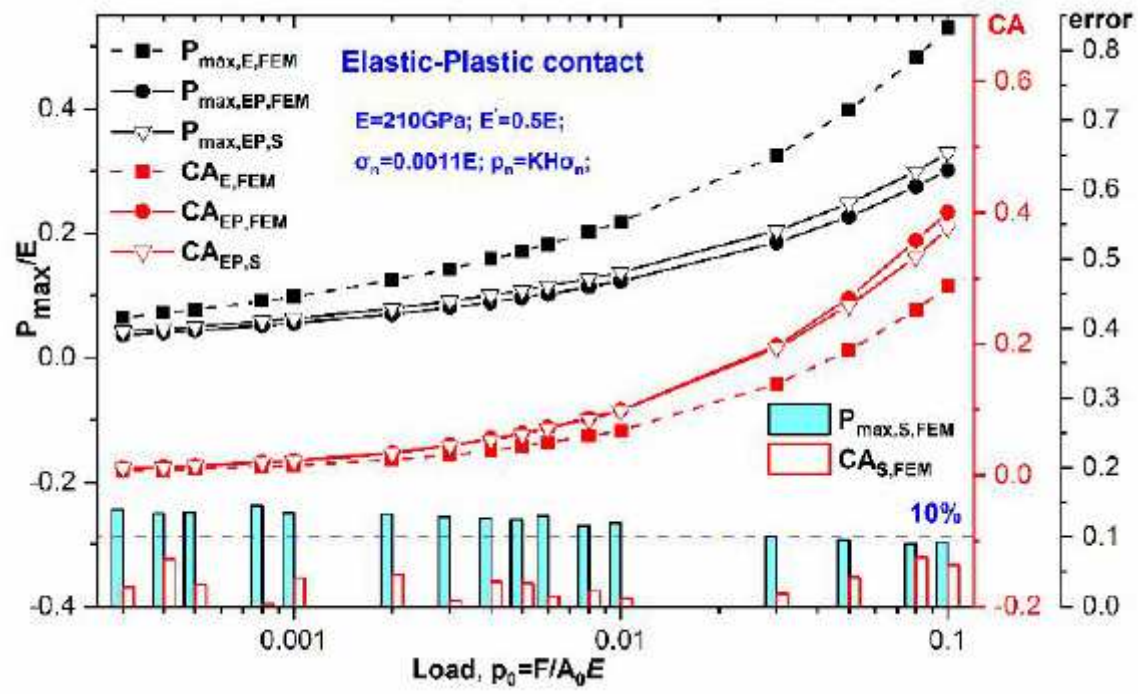

Figure 7

Results of elastoplastic contact by numerical method. 'Pmax,E,FEM', 'Pmax,EP,FEM', 'Pmax,EP,S' represent Pmax / E of elastic contact by FEM, elastoplastic contact by FEM and elastoplastic contact by numerical method. The representation of CA is similar. 'Pmax,S,FEM', 'CAS,FEM' are relative error of elastoplastic contact of numerical method and FEM.

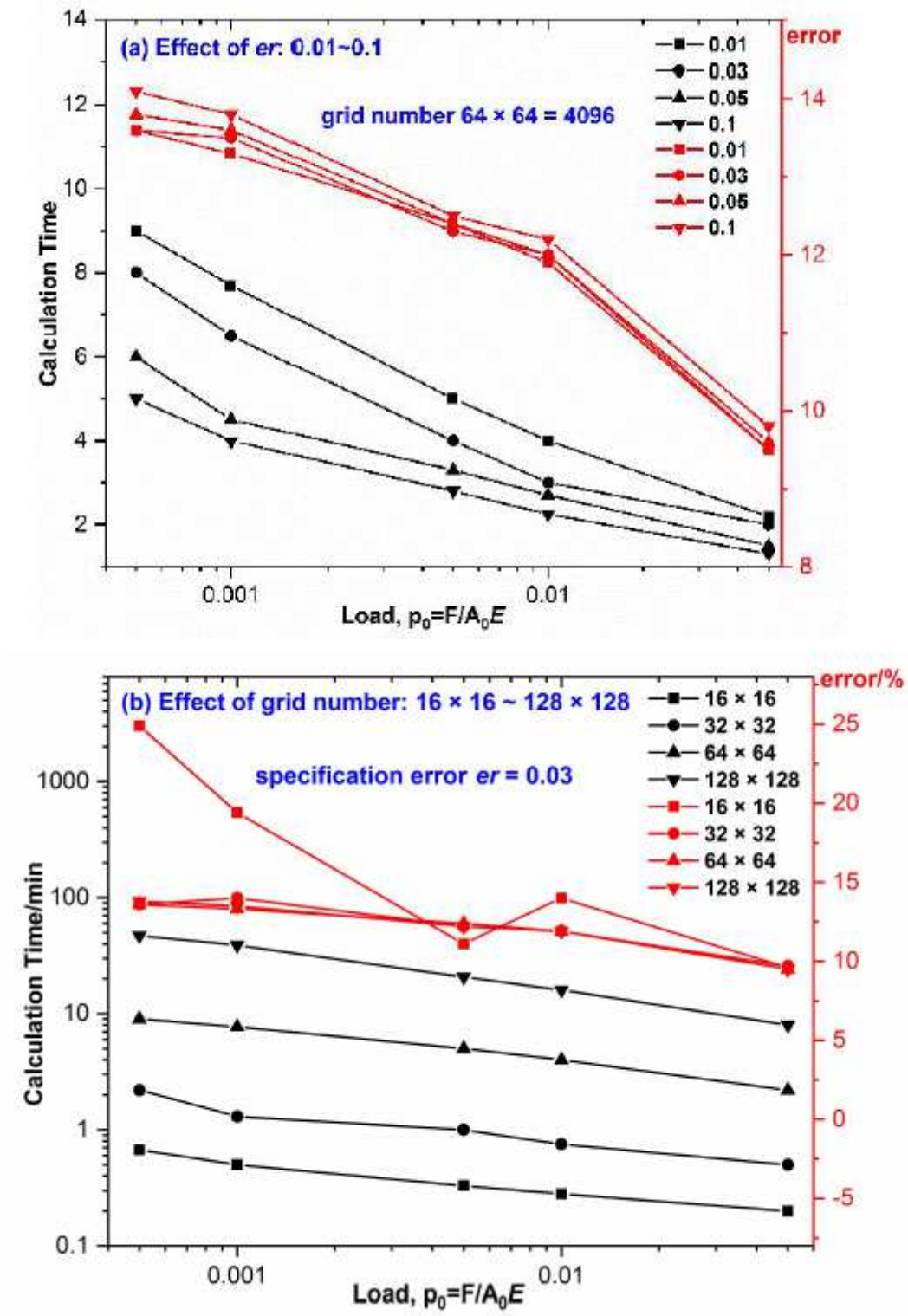

Figure 8

Calculation results under different er and different grid number. (a) Calculation results under different er. (b) Calculation results under different grid number.

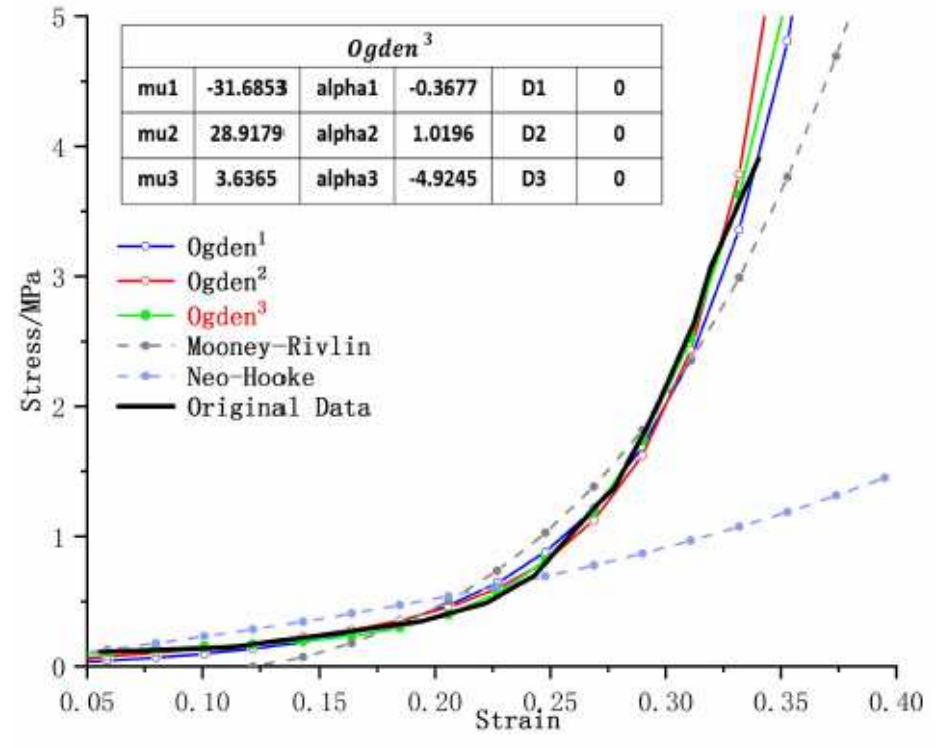

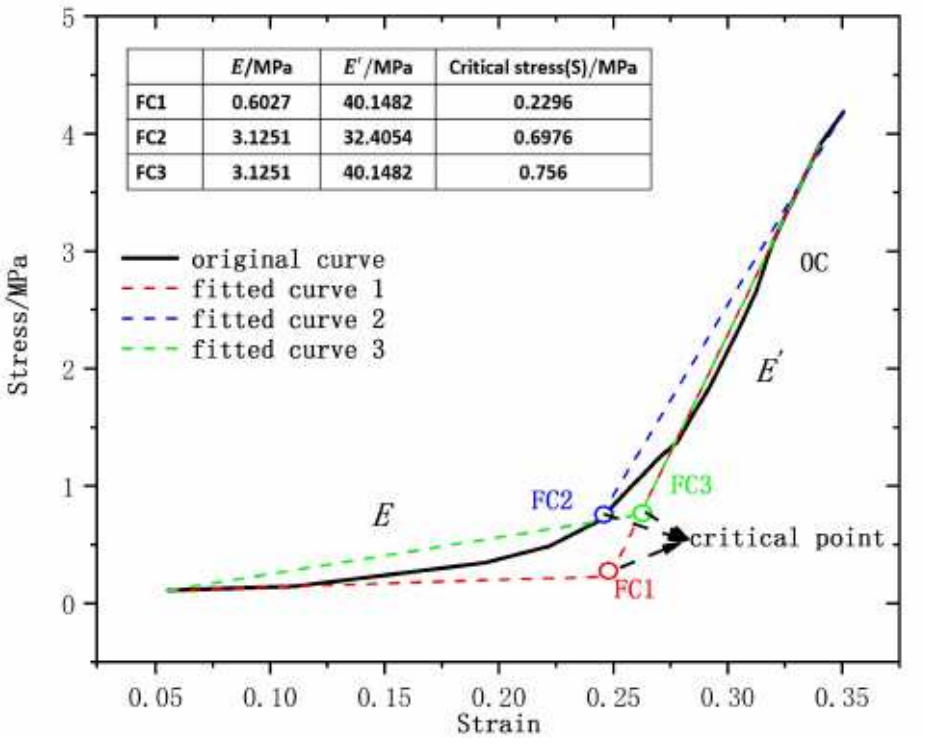

Figure 9

Fitting results of compressive stress-strain curve of material. (a) Constitutive model fitting of rubber for FEM. (b) Simplification of stress-strain curve for numerical method.

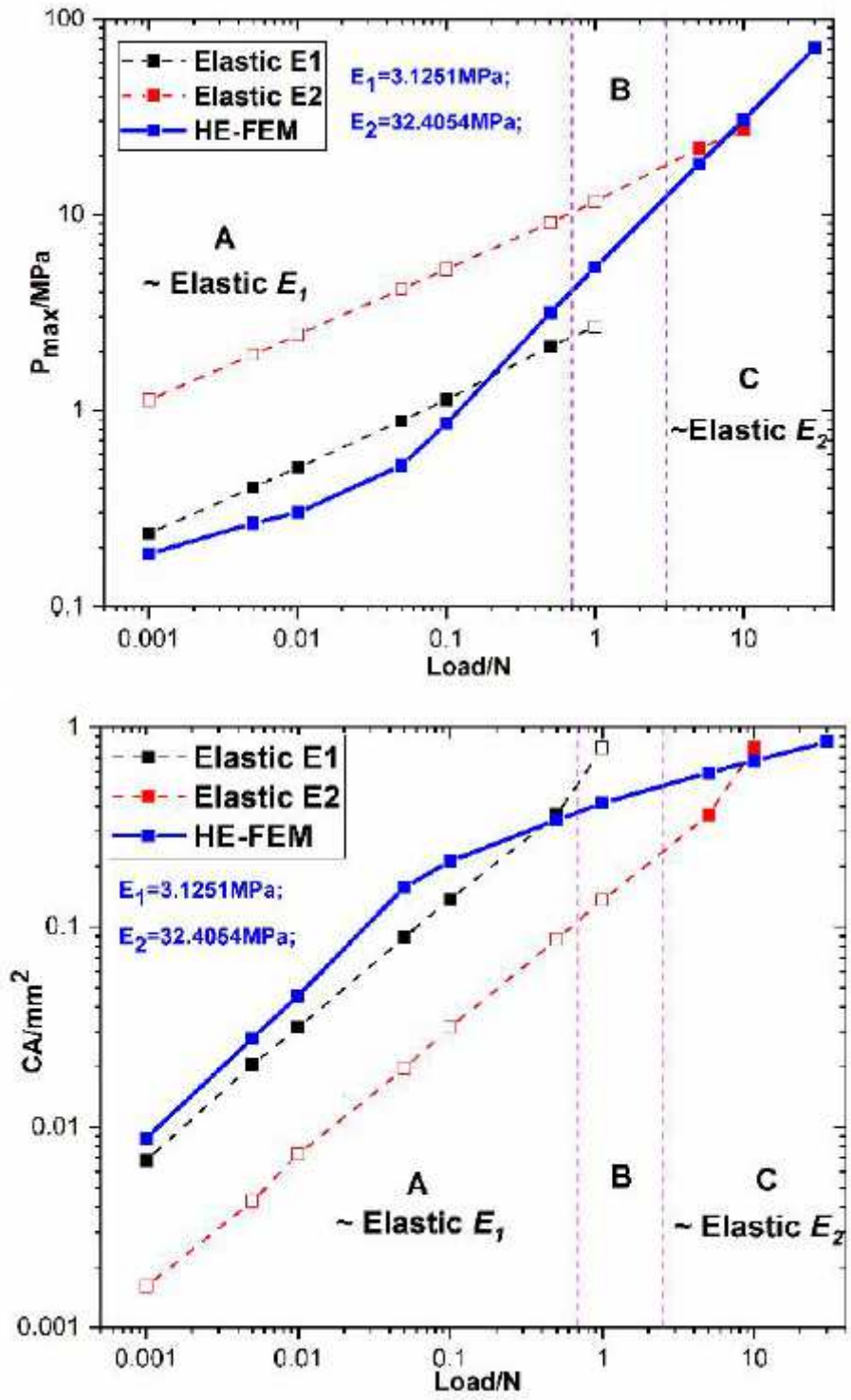

Figure 10

Results of hyperelastic contact and approximation by linear elastic contact calculation in FEM. 'Elastic E1', 'Elastic E2' represent the linear elastic contact results in FEM with elastic modulus E1 and E2, respectively. 'HE-FEM' represents the results of hyperelastic contact calculation in FEM. (a) Variation in the maximum contact pressure Pmax with load. (b) Variation in dimensionless contact area CA with load.

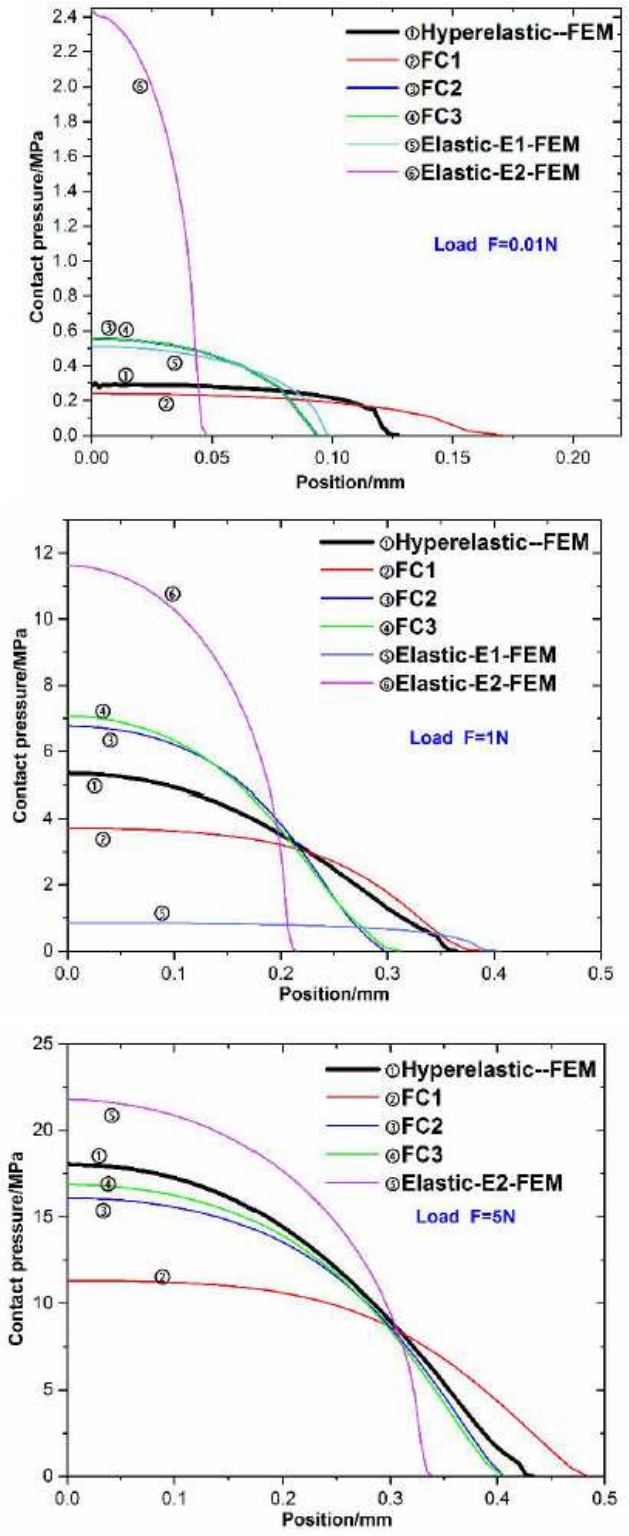

Figure 11

Pressure distribution along the radius of contact area. 'Hyperelastic–FEM' represents the result of hyperelastic contact calculation in FEM. 'FC1', 'FC2', 'FC3' represent the results of non-linear elastic contact calculation with fitted curves FC1, FC2 and FC3 in numerical method, respectively. 'Elastic-E1-FEM' and 'Elastic-E2-FEM' represent the results of elastic contact calculation with elastic modulus of E1

and E2 in FEM, respectively. (a) Pressure distribution under load of 0.01 N. (b) Pressure distribution under load of 1 N. (c) Pressure distribution under load of 5 N.

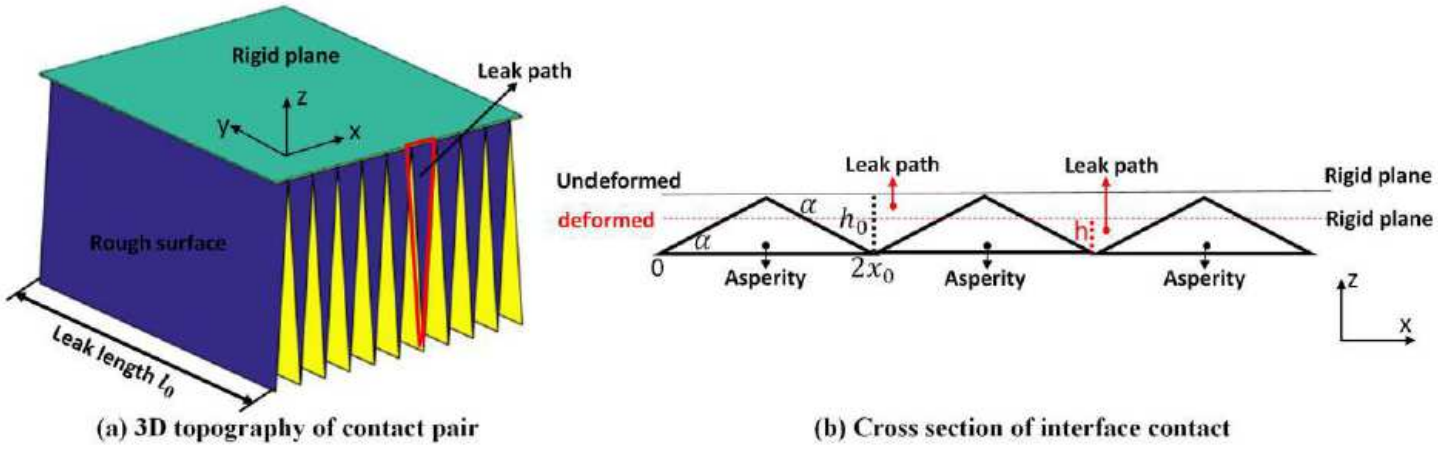

(a) 3D topography of contact pair

(b) Cross section of interface contact

Figure 12

The contact between the machined rough surface and the rigid plane.

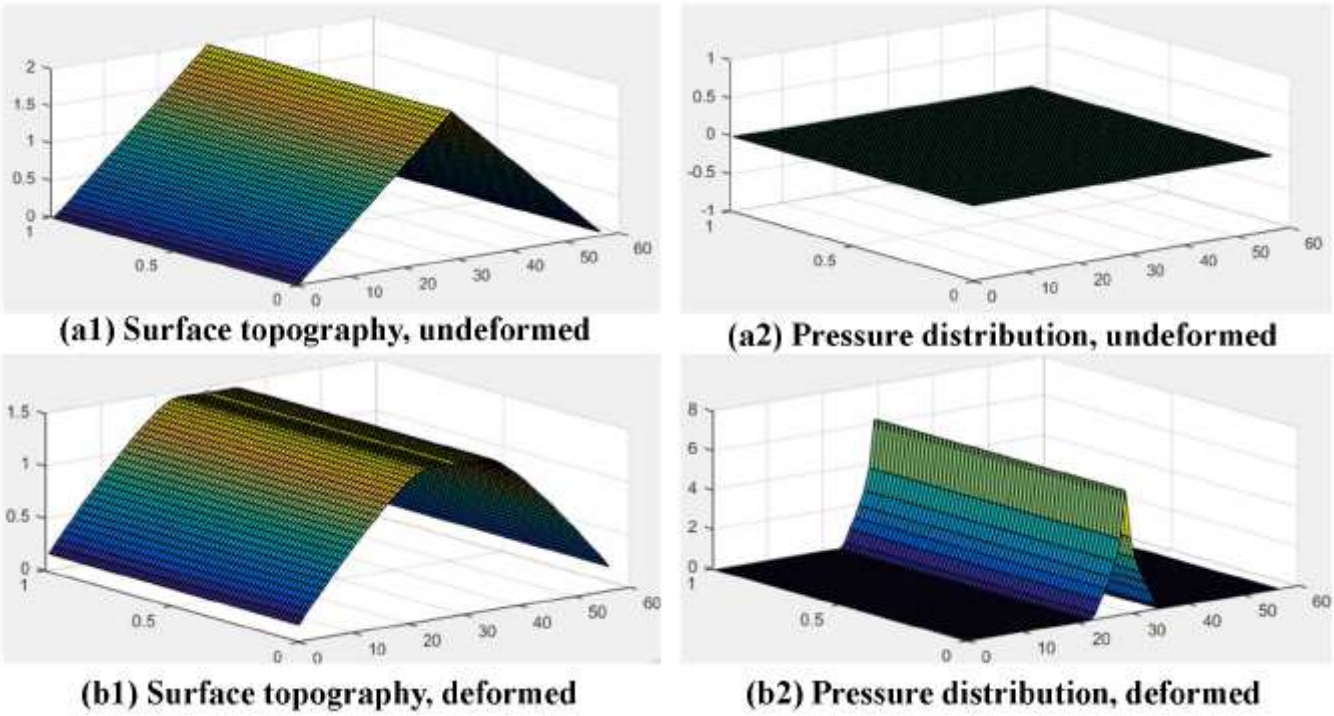

(a1) Surface topography, undeformed

(a2) Pressure distribution, undeformed

(b1) Surface topography, deformed

(b2) Pressure distribution, deformed

Figure 13

Surface topography and pressure distribution of undeformed and deformed condition. p0=0.5. Take elastic contact calculation as an expamle, the results of elastoplastic and hyperelastic contact are similar.

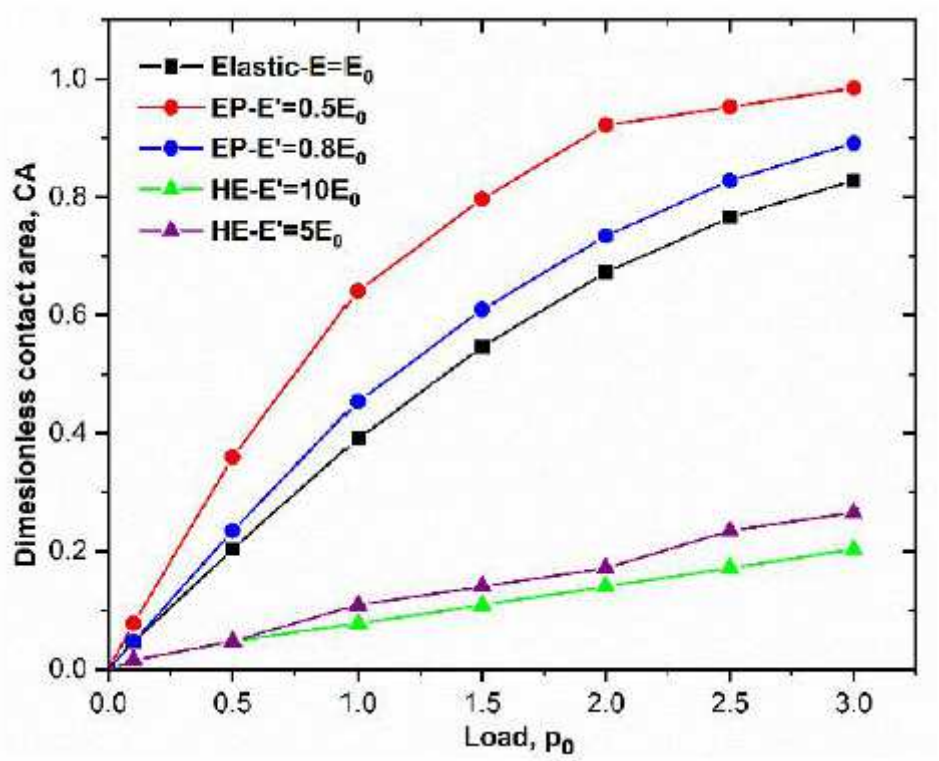

Figure 14

Dimensionless contact area CA with different materials.

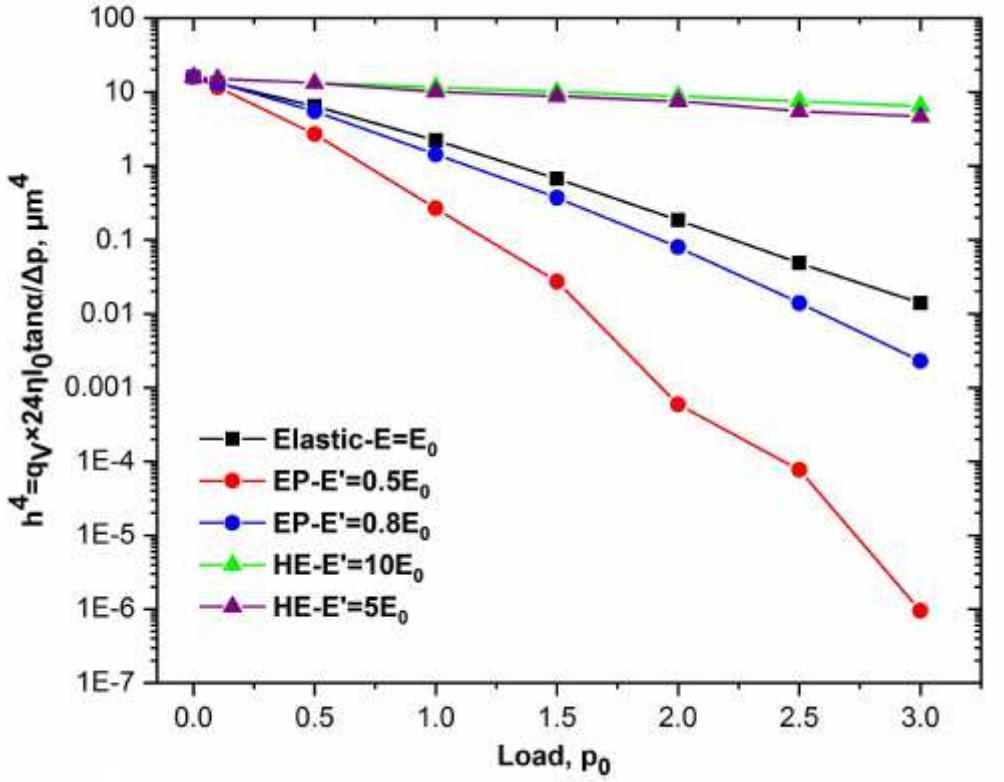

Figure 15

Volume flow rate with different materials.

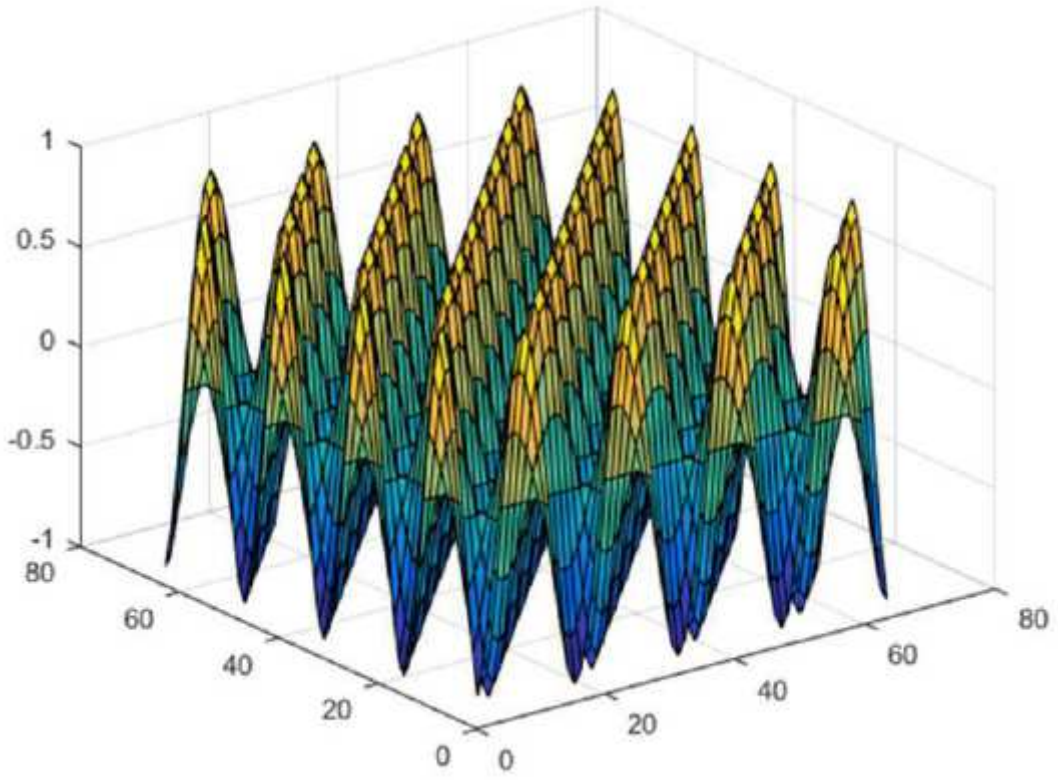

Figure 16

The topography of undeformed rough surface.

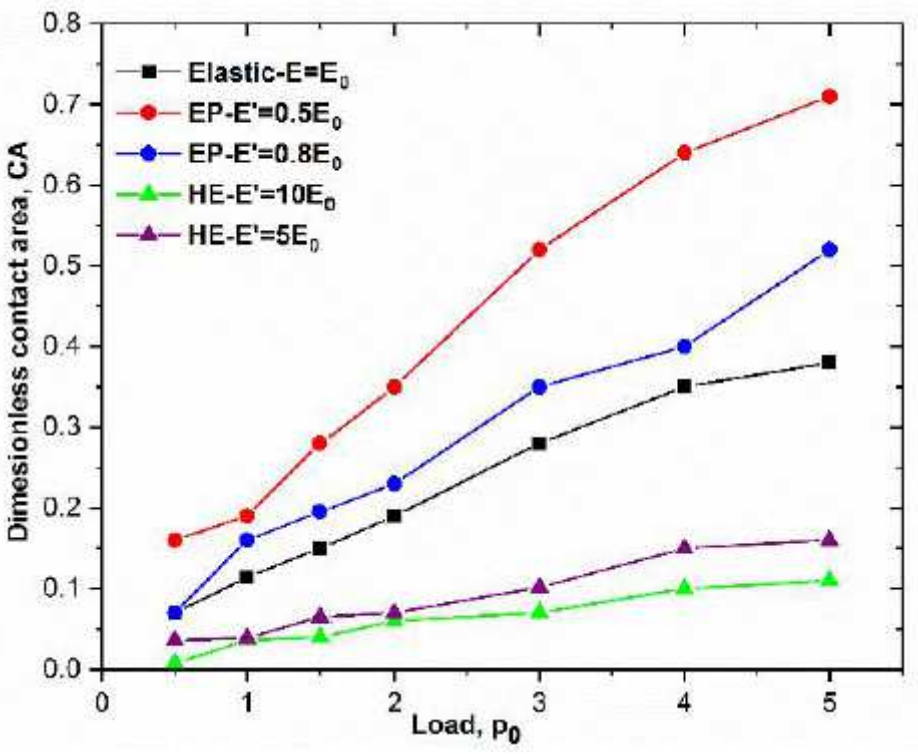

Figure 17

Dimensionless contact area CA with different materials.

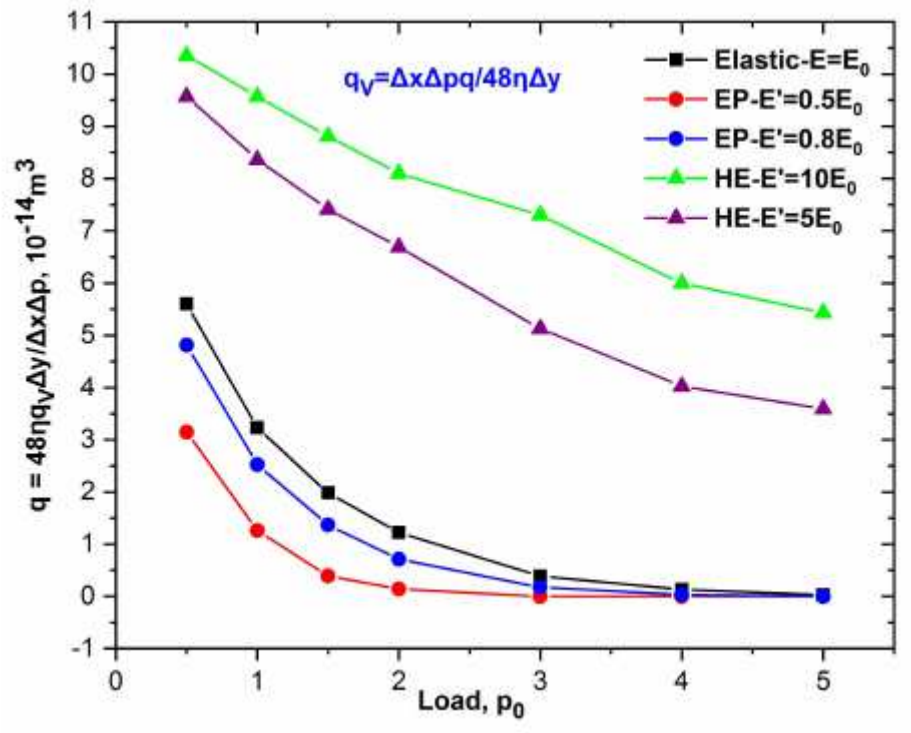

Figure 18

Volume flow rate with different materials.

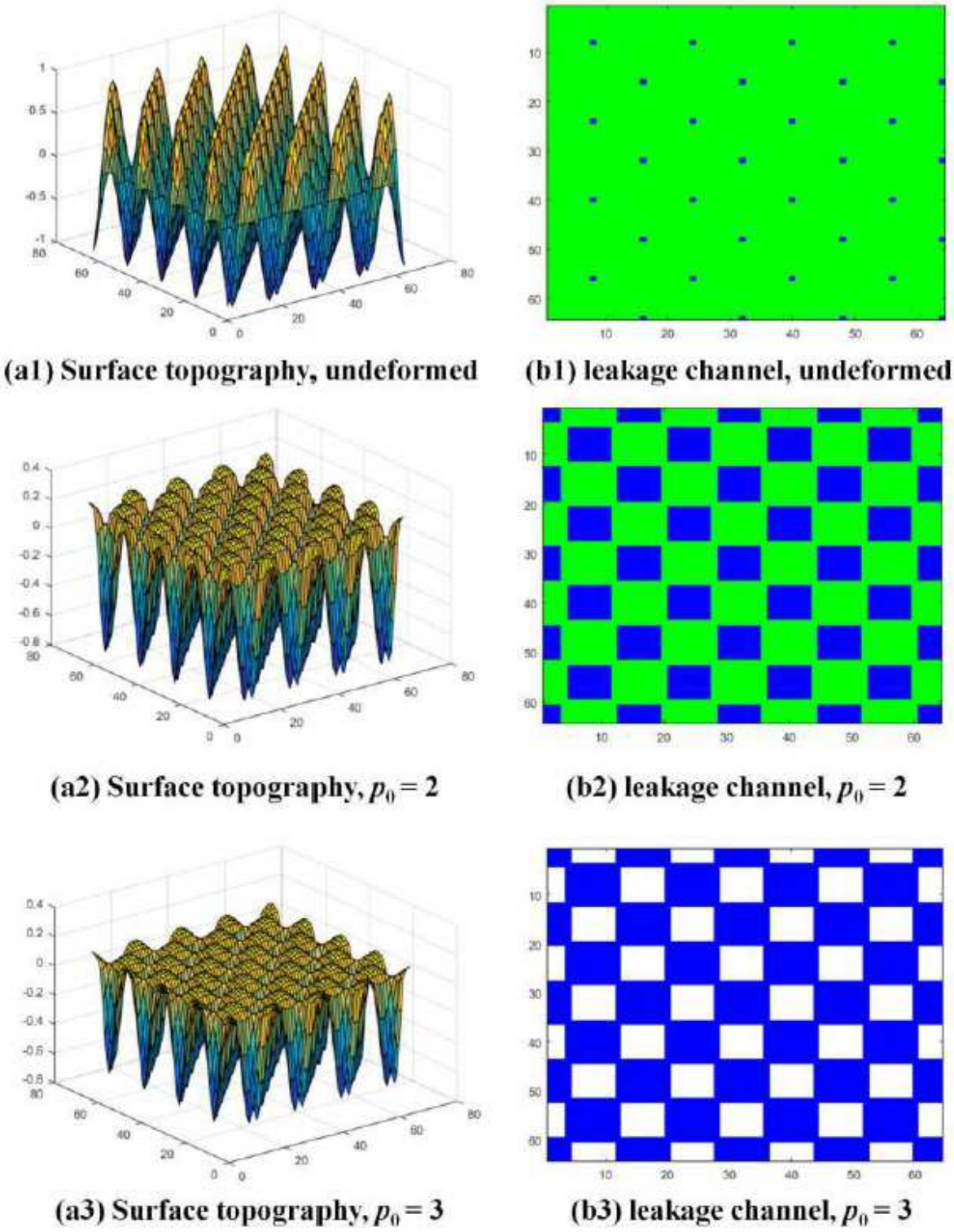

Figure 19

Surface contact state evolution of elastoplastic contact with E' = 0.5 E.